OPEN ACCESS
CellPress

Cell Reports
Article

A Mitochondrial Switch Promotes Tumor Metastasis

Paolo E. Porporato,[1] Valéry L. Payen,[1] Jhudit Pérez-Escuredo,[1] Christophe J. De Saedeleer,[1] Pierre Danhier,[2] Tamara Copetti,[1] Suveera Dhup,[1] Morgane Tardy,[1] Thibaut Vazeille,[1] Caroline Bouzin,[1] Olivier Feron,[1] Carine Michiels,[3] Bernard Gallez,[2] and Pierre Sonveaux[1,*]

[1]Institut de Recherche Expérimentale et Clinique (IREC), Pole of Pharmacology (FATH), Université catholique de Louvain (UCL), Brussels 1200, Belgium

[2]Louvain Drug Research Institute (LDRI), Biomedical Magnetic Resonance Research Group (REMA), Université catholique de Louvain (UCL), Brussels 1200, Belgium

[3]URBC-NARILIS, University of Namur, Namur 5000, Belgium

*Correspondence: pierre.sonveaux@uclouvain.be

http://dx.doi.org/10.1016/j.celrep.2014.06.043

SUMMARY

Metastatic progression of cancer is associated with poor outcome, and here we examine metabolic changes underlying this process. Although aerobic glycolysis is known to promote metastasis, we have now identified a different switch primarily affecting mitochondria. The switch involves overload of the electron transport chain (ETC) with preserved mitochondrial functions but increased mitochondrial superoxide production. It provides a metastatic advantage phenocopied by partial ETC inhibition, another situation associated with enhanced superoxide production. Both cases involved protein tyrosine kinases Src and Pyk2 as downstream effectors. Thus, two different events, ETC overload and partial ETC inhibition, promote superoxide-dependent tumor cell migration, invasion, clonogenicity, and metastasis. Consequently, specific scavenging of mitochondrial superoxide with mitoTEMPO blocked tumor cell migration and prevented spontaneous tumor metastasis in murine and human tumor models.

INTRODUCTION

Tumors are highly heterogeneous in all phenotypic features including glucose metabolism. Although glycolysis is coupled to oxidative phosphorylation (OXPHOS) in oxygenated tumor cells, some malignant cells are subject to fluctuations in oxygen availability and, therefore, rely on glycolysis uncoupled from OXPHOS for energy production (Dewhirst, 2009). From an energetic standpoint, it is surprising that some cancer cells also perform aerobic glycolysis (known as the Warburg effect), characterized by an increased normoxic flux of glucose to lactate (Warburg, 1956). However, this particular metabolic phenotype is shared with nonmalignant proliferating cells and is therefore thought to reflect increased biosynthetic plasticity (Vander Heiden et al., 2009; Ward and Thompson, 2012). Although it sometimes results from mutations (Frezza et al., 2011), there is evidence that mitochondria generally retain full oxidative capacities in solid tumors and that aerobic glycolysis can often be reverted (Faubert et al., 2013; Vaupel and Mayer, 2012), suggesting that this metabolic activity generally results from reversible changes that could be targeted pharmacologically. Thus, mitochondria actively contribute to aerobic glycolysis by producing cataplerotic intermediates and reducing equivalents to sustain cell growth and cell cycling (Anastasiou et al., 2011; Vander Heiden et al., 2009).

Tumor metastasis is a leading cause of cancer death. The metastatic switch marking the onset of metastatic dissemination corresponds to the acquisition of specific traits by tumor cells, including migration, invasion, and survival in the blood stream (Gupta and Massagué, 2006; Roussos et al., 2011). Three main lines of evidence led us to hypothesize that metastasis is under metabolic control. First, PET with the glucose analog tracer [18]-F-fluorodeoxyglucose (FDG) is routinely used for the clinical detection and imaging of tumor metastasis (Gambhir et al., 2001). This application is based on the observation that the vast majority of metastases trap far more glucose than normal tissues (with the exception of the brain), which has often been related to metabolic characteristics already acquired at the primary tumor site (Vander Heiden et al., 2009). Second, aerobic glycolysis could offer protection against oxidative damage and cell death when tumor cells transit in oxygenated blood (Porporato et al., 2011). Third, a mitochondrial defect corresponding to an inactivating mutation of respiratory chain complex I has been found in a metastatic mouse Lewis lung carcinoma cell line and was absent in weakly metastatic parental cells (Ishikawa et al., 2008a). Experimentally, the transfer of mtDNA from highly to weakly metastatic cells increased their metastatic potential in mice.

It is estimated that on average 10^6 tumor cells per gram of tumor are shed in the circulation daily (Chang et al., 2000). Of these cells, only a few, termed metastatic progenitors, are able to generate metastases in distant organs. In this study, we tested whether Warburg-phenotype tumor cells constitute a population of metastatic progenitors. We observed that tumor cell migration, invasion, clonogenicity, metastatic take, and spontaneous metastasis in mice are promoted by the natural selection of a mitochondrial phenotype associated with superoxide production, which was phenocopied by experimentally targeting the electron transport chain (ETC). We also report that pharmacological scavenging of mitochondrial superoxide prevents metastatic dissemination from primary orthotopic tumors in mice.

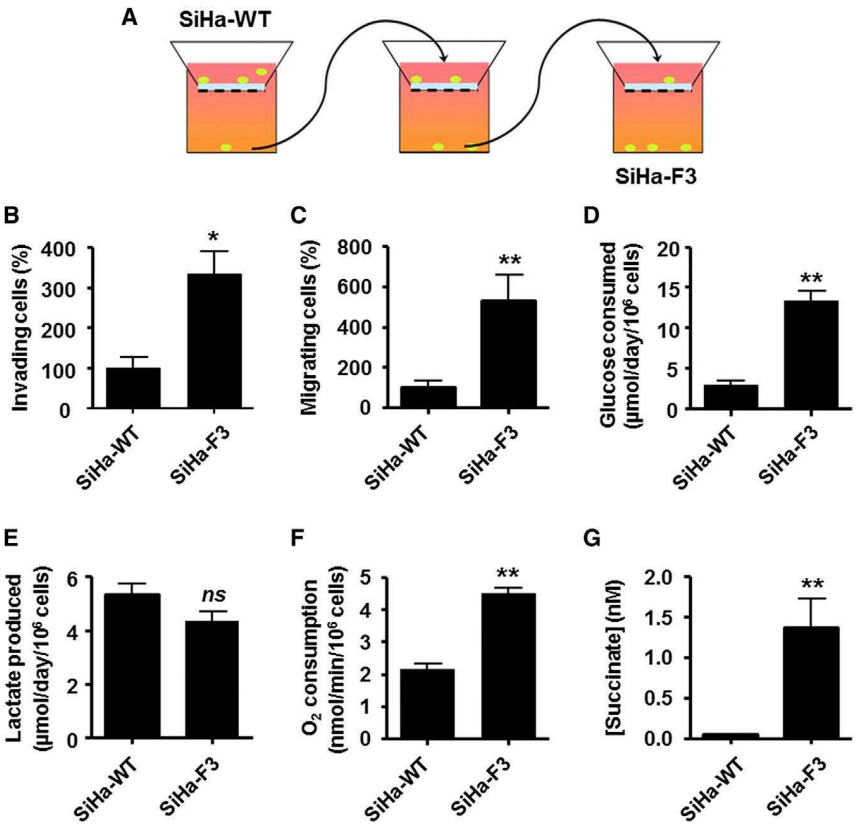

Figure 1. The Experimental Selection of Superinvasive Tumor Cells Correlates with Increased Mitochondrial Activity

(A–C) SiHa-F3 cells were isolated from a total population of WT SiHa tumor cells following three consecutive rounds of in vitro invasion in Matrigel-coated transwells (model shown in A). Comparative (B) invasion and (C) migration assays (n = 3).

(D and E) Glucose consumption (D) and lactate production (E) over 24 hr (n = 3).

(F) Mitochondrial oxygen consumption of adherent cells (n = 8).

(G) Intracellular succinate levels (n = 5).

All data represent means ± SEM. *p < 0.05, **p < 0.01, ***p < 0.005, ns, not significant compared to SiHa-WT by Student's t test.

RESULTS

In Vitro Selection of Superinvasive Tumor Cells Coselects Increased Mitochondrial Activity

To test the contribution of glycolysis to tumor metastasis, we first used a correlative approach in vitro. Invasion is a fundamental characteristic of metastatic tumor cells (Nguyen et al., 2009). A wild-type (WT) population of oxidative SiHa human cervix squamous cell carcinoma cells (Sonveaux et al., 2008) was subjected to three rounds of in vitro selection (Figure 1A) resulting in the isolation of SiHa-F3 cells with enhanced invasive activity (Figure 1B). The cells, which had also gained an increased migratory phenotype (Figure 1C), were analyzed for glucose metabolism. They were characterized by an enhancement of glucose uptake that was surprisingly not associated with higher lactate production (Figures 1D and 1E). Adherent SiHa-F3 cells showed increased mitochondrial O_2 consumption (Figure 1F) and succinate accumulation (Figure 1G) compared to WT cells.

In Vivo Selection of Supermetastatic Tumor Cells Coselects for Increased Levels of TCA Intermediates

The above model was instrumental in postulating the existence of a metabolic phenotype associated with tumor metastasis, which was confirmed in vivo with mouse melanoma tumor cells. B16F10 cells, which are only moderately metastatic in spontaneous assays (Brown et al., 2002), were subjected to rounds of in vivo selection for increased metastatic activity (Figure 2A). B16-M1 to M5 tumor cells were expanded after one to five rounds of selection, with two parallel selections producing two distinct populations of metastatic cells, M2/3a and M4/5b. As shown for B16-M4b in Figure 2B, in vivo selection significantly enhanced spontaneous metastatic activities to the lungs. Selected cells had also gained improved invasiveness (Figure 2C) and clonogenicity (Figure 2D). Clonogenicity, in particular, was increased upon selection compared to the weakly metastatic B16F10 and the nonmetastatic B16F1 variants (Fidler, 1975). From a metabolic standpoint, we found no difference in the rate of glucose uptake and lactate release (Figure 2E) and mitochondrial oxygen consumption (Figure 2F) when comparing adherent B16F10 to B16-M2a and B16-M4b. Cells freshly isolated from primary tumors generated with B16F10 served to verify that in vivo implantation did not account for changes (Figure 2E). Although the glycolytic flux and oxygen consumption were unchanged, we detected increased succinate (Figure 2G) and 2-oxoglutarate (Figure S1A) production in supermetastatic cells, suggesting a TCA dysfunction. Compared to B16F10, B16-M4b possessed larger mitochondria with numerous cristae (Figure 2H). This mitochondrial phenotype did not influence ATP levels (Figure 2I) and tumor cell proliferation (Figure S1B). The relative contribution of OXPHOS to ATP synthesis was tested by adding rotenone, and the contribution of glycolysis under hypoxic conditions; no difference was found between B16F10 and B16-M4b cells (Figure 2I). Collectively, these data provide a positive correlation between the metastatic activities of cancer cells and a mitochondrial switch corresponding to aberrant TCA cycle activity, similar to what we found in superinvasive SiHa cells (Figure 1).

Partial Electron Transport Chain Inhibition Promotes Tumor Cell Migration

To provide direct evidence of a mitochondrial contribution to tumor metastasis in our models, we first generated ρ0 cells with

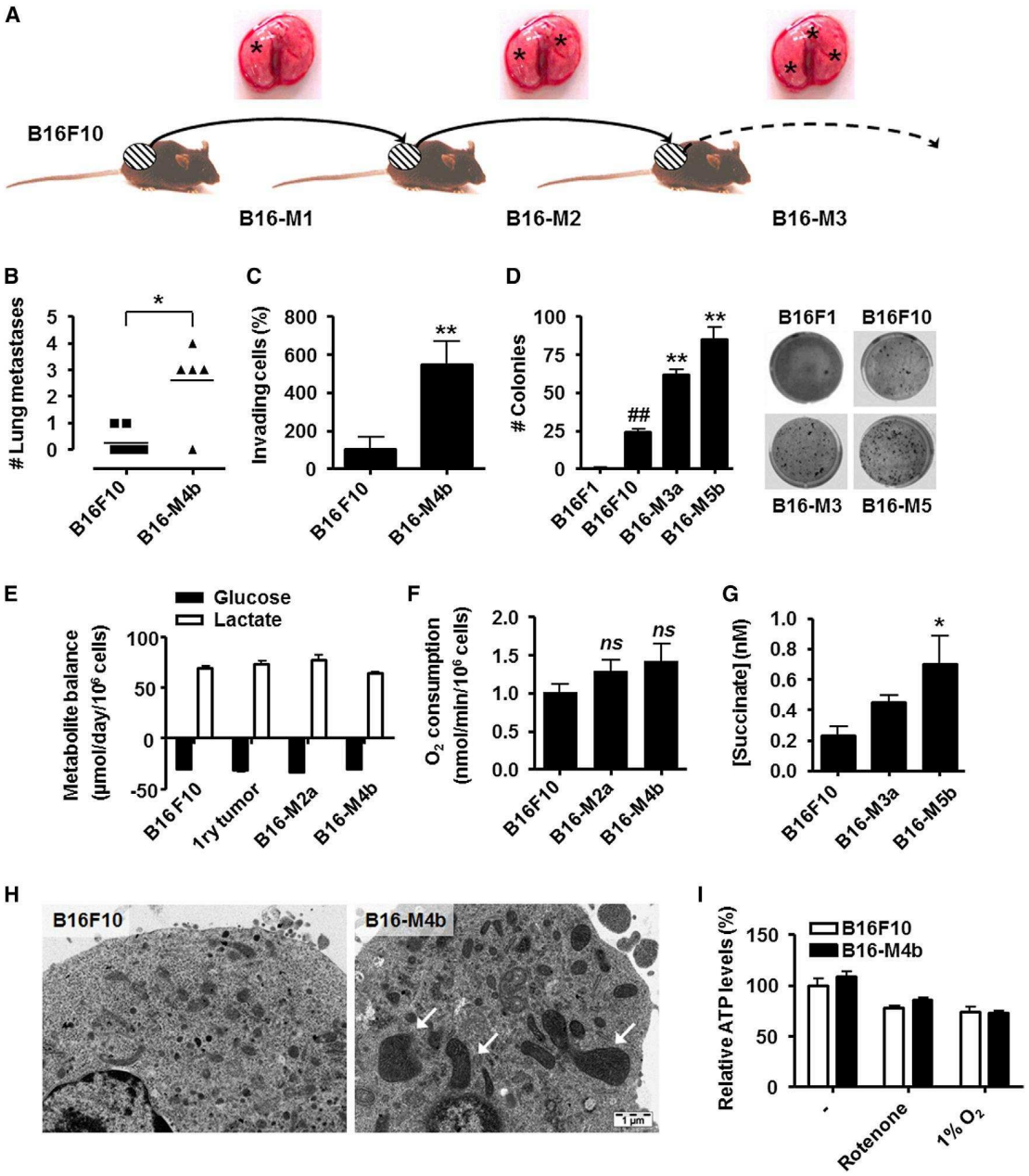

Figure 2. The Experimental In Vivo Selection of Supermetastatic Tumor Cells Is Associated with a TCA Cycle Overload

(A) B16-M1 to B16-M5 cells were, respectively, retrieved after one to five rounds of in vivo selection for lung metastasis from a primary subcutaneous tumor initially generated with B16F10 tumor cells (model shown in A, where expected lung metastasis density is represented by asterisks).

(B) Spontaneous lung metastasis detected 30 days after the subcutaneous implantation of a primary tumor ($n \geq 5$).

(C) Overnight in vitro invasion assay ($n = 6$).

(D) Colony formation assay ($n = 3$).

(E) Glucose consumption and lactate production over 24 hr ($n = 4$).

(F) Mitochondrial oxygen consumption of adherent cells ($n = 8$).

(G) Intracellular succinate levels ($n = 4$).

(H) Representative electron microscopy pictures. Arrows indicate giant mitochondria. Bar, 1 µm.

(I) Intracellular ATP levels after 8 hr of culture with the indicated treatments.

All data represent means ± SEM. *$p < 0.05$, **$p < 0.01$, ***$p < 0.005$, ns, not significant compared to B16F10; $^{\#\#}p < 0.01$ compared to B16F1, by Student's t test (B and C) or one-way ANOVA (D–G and I). See also Figure S1.

dysfunctional mitochondria (Sonveaux et al., 2008). SiHa-ρ0-D2 cells, further subcloned from the total SiHa-ρ0 population, were devoid of intact mitochondria (Figure S2A). Compared to WT, SiHa-ρ0 and SiHa-ρ0-D2 showed partial and total impairment of mitochondrial respiration, respectively (Figure 3A). It was coherent with a progressive decline in mitochondria-encoded cytochrome *c* oxidase I (mt-CO1 protein expression, Figure S2B), and glycolytic compensation (Figure 3B). In vitro assays revealed increased migratory (Figure 3C) and invasive (Figure 3D) activities of SiHa-ρ0 compared to WT. Strikingly, in the same experimental conditions, SiHa-ρ0-D2 showed a close to complete impairment of migration and invasion compared to SiHa-ρ0 and WT cells (Figures 3C and 3D). These experiments were key in showing that mitochondria must be present, active but dysfunctional, to promote the migratory phenotype. We therefore aimed to identify the nature of possible dysfunctions with more accurate approaches.

Others previously reported that mutations partially inactivating ETC complex I and associated with increased mitochondrial reactive oxygen species (mtROS) production can promote tumor metastasis (Ishikawa et al., 2008a). To go beyond these findings, we reasoned that any intervention bottlenecking the ETC could promote tumor cell migration, which was tested with WT SiHa cells in transwells. Accordingly, low-dose rotenone (targeting respiration complex I; Sherer et al., 2003), 3-nitropropionate (3-NP, inhibiting respiratory complex II; Maciel et al., 2004), and a partial knockdown of *mt-CO1* (complex IV; Tsukihara et al., 1996; Figure S2C) all highly significantly promoted SiHa cell migration (Figure 3E). Moderate complex III inhibition also enhanced tumor cell migration (tested in the B16 model, detailed after). That partial ETC inhibition promotes tumor cell migration was confirmed using 4T1 mouse mammary carcinoma cells treated with rotenone (Figure S2D). Rotenone also allowed us to identify the existence of a phenotypic window, with doses ranging from 1 to 100 nM promoting SiHa tumor cell migration, whereas doses lower than 1 nM or higher than 100 nM did not (Figure 3F). It is of note that rotenone below 1 nM would have little or no pharmacological effect and at 1 μM would typically cause full respiration blockade (Brown and Nurse, 2008).

Mitochondrial ROS Promote and mitoTEMPO Inhibits Tumor Cell Migration

Partial ETC inhibition may result in incomplete oxygen reduction to yield superoxide (Brandon et al., 2006), a precursor of other promigratory ROS (Cannito et al., 2010). Accordingly, rotenone at a dose of 10 nM optimally promoting migration (Figure 3F) also enhanced mitochondrial superoxide production in WT SiHa cells, as detected with mitoSOX (Zhou et al., 2011; Figure 3G). MitoSOX was not sensitive enough to show increased superoxide production by other ETC inhibitors; we therefore tested mtROS contribution with specific antioxidants in migration assays (Tsukihara et al., 1996). We first found that *N*-acetyl-*L*-cysteine (NAC) totally inhibited the promigratory effects of ETC bottlenecking (Figure 3E). It did not impact basal cell migration. Similar to NAC, the H_2O_2 scavenger Ebselen (Schewe, 1995) had no basal effect but countered the induction of SiHa cell migration by rotenone and *mt-CO1* inhibition (Figure 3H). Involvement of upstream mitochondrial superoxide was probed with mitoTEMPO, a specific scavenger of mitochondrial superoxide (Dikalova et al., 2010; Nazarewicz et al., 2013a). MitoTEMPO recapitulated the effects of Ebselen in the same assays (Figure 3I), whereas methyltriphenylphosphonium (mTPP), used as a control, did not prevent rotenone-induced SiHa cell migration (Figure S2E). Together, our data pointed toward mtROS as key molecular intermediates enhancing tumor cell migration upon partial ETC inhibition.

If mtROS promoted the migration of cells with dysfunctional mitochondria, it would also confer a migratory phenotype to naturally selected tumor cells with dysfunctional TCA cycle activity. To test this hypothesis, we used SiHa-F3 and B16-M4b cells. We first found that, compared to their WT counterparts, both SiHa-F3 (Figure 3J, left panel) and B16-M4b (Figure 3K, left panel) had increased ROS levels (measured with CM-H_2DCFDA). Ebselen and mitoTEMPO were equally efficient in reverting the migratory phenotype acquired upon selection in vitro (SiHa-F3, Figure 3J, right panel) and in vivo (B16-M4b, Figure 3K, right panel). Both drugs also totally suppressed the enhanced migratory activity of SiHa-ρ0 that produced more ROS compared to WT cells (Figure 3L). These data collectively demonstrate that the migratory phenotype conferred by natural selection or by the experimental induction of partial ETC inhibition can be totally blocked by specific antioxidants.

Src Mediates Mitochondrial Superoxide-Dependent Tumor Cell Migration by Activating Focal Adhesion Kinase Pyk2

Several pathways could transduce promigratory mtROS signals. To identify a relevant effector, we performed a whole-genome microarray comparing rotenone-treated B16F10, B16-M2a, and B16-M4b to untreated B16F10 cells. A shared gene signature was identified that comprised 27 upregulated and 49 repressed genes (Table S1), among which focal adhesion kinase (FAK) family member *Ptk2b*/*Pyk2*, known to promote metastasis downstream of Src (Wendt et al., 2013), was induced. There was no shared signature of hypoxia-inducible factor-1 (HIF-1). We therefore focused on Src and Pyk2, previously reported to be ROS inducible (Cheng et al., 2002) but for which information is still missing regarding responsiveness to mtROS in particular (Graham et al., 2012; Lluis et al., 2007). We found that low-dose rotenone activates Src (Y416 phosphorylation) in the mitochondrial fraction of B16F10 cells, which was blocked by mitoTEMPO (Figure 4A). MitoTEMPO also decreased mitochondrial Src phosphorylation in B16-M4b cells (Figure 4B). Downstream, *Pyk2* transcription and Pyk2 protein expression and activity (Y402 phosphorylation) were increased in B16-M4b compared to B16F10 cells, and all responses were repressed by mitoTEMPO (Figure 4C). Of note, Pyk2 phosphorylation preceded its expressional induction, which was evidenced using low dose rotenone (Figure 4D), and the effects of rotenone were also mitoTEMPO sensitive. That Src lies upstream of Pyk2 in mtROS signaling was established by showing that Src inhibitor PP1 repressed Pyk2 protein expression in B16-M4b and in rotenone-treated B16F10 cells (Figure 4E). Based on a previous report linking Src to

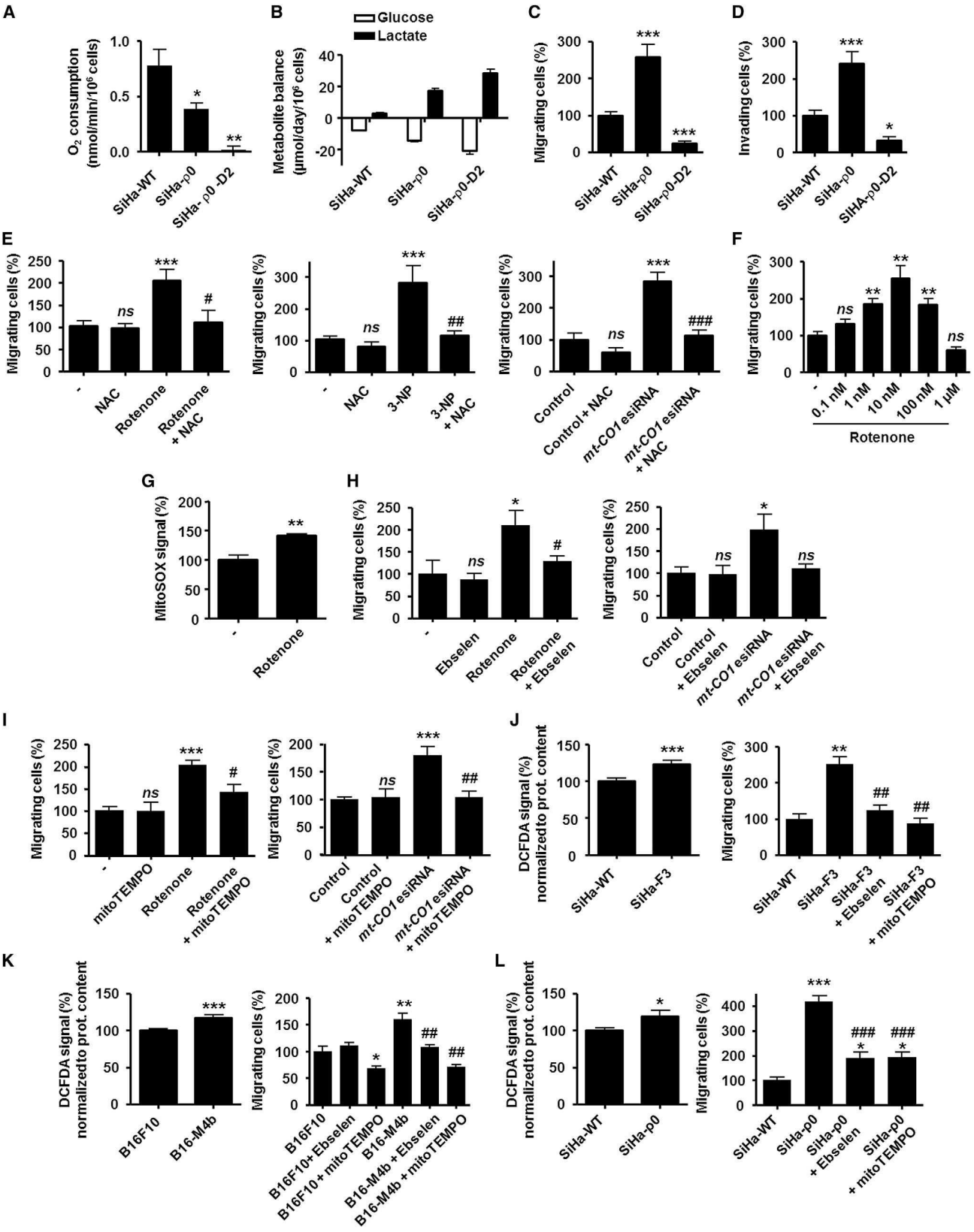

(legend on next page)

SMAD activation (Wendt et al., 2013), we further found that Pyk2 protein induction by mtROS involves transcriptional factors SMADs as it was repressed by an endoribonuclease-prepared small interfering RNA (esiRNA) against *SMAD4* (Figures 4F and S3A).

Next, we phenotypically linked the mtROS-Src-Pyk2 pathway to tumor migration. Indeed, Src inhibitor PP1 blocked the migratory phenotype of B16-M4b and of rotenone-treated B16F10 cells (Figure 4G), and SMARTpool *Pyk2*-specific siRNAs had the same effect (Figure 4H; see Figure S3A for target extinction). Coherently, the migratory phenotype of SiHa-F3 cells was also abolished by PP1 and *Pyk2* siRNA (Figures 4I and S3A) and with the dual Pyk2/FAK inhibitor PF431396 (Figure S3B). Similar responses were documented for SiHa-ρ0 cells (Figures S3A–S3C). In naturally highly metastatic MDA-MB-231 human breast cancer cells, Pyk2 also highly significantly contributed to cell migration, and its expression was repressed by mitoTEMPO (Figures S3A, S3D, and S3E). Altogether, these data evidence that activation of Src-Pyk2 signaling by mtROS promotes tumor cell migration, which can be targeted with the specific mitochondrial superoxide scavenger mitoTEMPO.

Mitochondrial ROS Scavenging Prevents Metastatic Take in Mice

In the ETC, complexes I and III are the main sources of electron leakage, hence of superoxide (Muller et al., 2004). To extend the scope of our findings to metastatic hallmarks other than migration, we first focused on complex I. Compared with untreated cells, B16F10 cells treated with low-dose rotenone showed increased in vitro invasion (Figure 5A) and clonogenicity (Figure 5B) within the concentration range previously found to stimulate migration without blocking respiration (see Figures 4B and S4A). These responses closely reproduced the metastatic features gained upon in vivo selection (Ishikawa et al., 2008a; see also Figures 2C and 2D). We therefore tested in vivo the consequences of tumor cell pretreatment with rotenone, and focused on upstream mtROS. Compared to control, a 6 hr pretreatment of B16F10 cells with 20 nM of rotenone (twice the optimal in vitro dose to take into account possible in vivo washout) significantly promoted metastatic take in lungs after tail vein injection in syngeneic mice (Figure 5C). An independent series of experiments using the same model not only confirmed this observation but further revealed that mitoTEMPO successfully prevented the prometastatic effect of rotenone (Figure 5D), a property that was not shared by mTTP (Figure S4B). The antimetastatic effects of mitoTEMPO were similar to those observed with Src inhibitor saracatinib (suitable for in vivo use according to Dong et al. [2010]; Figure S4C) and *Pyk2* small hairpin RNA (shRNA) (Figures S4D and S4E) in the same model, further illustrating the involvement of mtROS-Src-Pyk2 signaling in metastasis. It was confirmed with B16-M4b cells, because two different *Pyk2* shRNAs blocked metastatic take (Figures S4F and S4E).

To broaden the scope of our findings beyond specific effects of mitoTEMPO, we used mitoQ, a mitochondria-targeted form of coenzyme Q10 (Kelso et al., 2001). MitoQ inhibited the metastatic take of rotenone-pretreated B16F10 cells (Figure 5E), whereas negative control decyl-TPP (dTPP) did not. These data collectively demonstrate that mtROS promote metastatic take, which can be blocked pharmacologically.

Mitochondrial ROS Scavenging Prevents Spontaneous Tumor Metastasis in Mice

To test whether partial ETC inhibition also promotes spontaneous metastasis, we next focused on complex III. To this aim, we used two different shRNAs (shUQCRB-1 and shUQCRB-2) targeting ubiquinol-cytochrome *c* reductase binding protein (UQCRB; Haut et al., 2003). Compared to cells expressing a control shRNA (shCTR), those with partial target extinction (Figure S5A) showed a partial inhibition of mitochondrial O_2 consumption (Figure 6A) and increased Pyk2 mRNA and protein expression (Figure S5B), associated with increased in vitro migration (Figure 6B), invasion (Figure 6C), and clonogenicity (Figures 6D and S5C). These data validated the model to faithfully reproduce the phenotype of the B16-M variants selected in vivo (Figures 2 and 4). In addition, shUQCRB promoted both experimental (Figure S5D) and spontaneous (Figure 6E) B16F10 metastasis compared to shCTR.

Finally, we tested whether mitochondrial superoxide scavenging with mitoTEMPO could be used to prevent spontaneous tumor metastasis in vivo. We detected significantly less spontaneous lung metastases in the animals treated chronically with mitoTEMPO (0.7 mg/kg, daily i.p.) compared to vehicle (Figure 6F). The therapeutic relevance of our observations was further addressed in the orthotopic model of MDA-MB-231 human breast cancer cells in SCID mice. Ex vivo bioluminescence of lungs 60 days after mammary fat-pad tumor cell implantation revealed that mitoTEMPO totally prevented metastasis to the lungs (only background luminescence was detected) by otherwise spontaneously metastatic human tumors (Figure 6G). Of note, mitoTEMPO did not modify primary tumor growth (Figure S5E) and did not induce overt toxicity when delivered chronically to mice.

Figure 3. Moderate OXPHOS Inhibition Promotes Tumor Cell Migration via Mitochondrial Superoxide

(A–D) SiHa-ρ0-D2 is a subclone of mitochondria-deficient SiHa-ρ0 cells. (A) Rotenone-sensitive oxygen consumption (n = 3). (B) Glucose consumption and lactate production over 24 hr (n = 3). Overnight (C) migration and (D) invasion ($n \geq 6$).

(E–I) SiHa-WT cells. (E) Overnight migration ± partial OXPHOS inhibition with low-dose rotenone (10 nM, targeting complex I, n = 6), 3-nitropropionate (3-NP, 10 μM, complex II inhibitor, n = 6), or a specific esiRNA against complex IV subunit *mt-CO1* (n = 6, partial target extinction shown in Figure S2C) ± *N*-acetyl-*L*-cysteine (NAC, 5 mM). (F) As in (E) but with increasing doses of rotenone (n = 6). (G) Mitochondrial superoxide production measured using mitoSOX in FACS after a 6 hr treatment ± 10 nM of rotenone (n = 4). (H) Overnight migration ± rotenone (10 nM, 6 hr) or *mt-CO1* esiRNA ± antioxidant Ebselen (20 μM, n = 6). (I) As in (H) but using the mitochondria-targeted superoxide-specific scavenger mitoTEMPO (50 μM) instead of Ebselen (n = 6).

(J–L) ROS production determined with CM-H_2DCFDA (left, $n \geq 8$) and overnight migration (right, n = 6 all) of cells ± Ebselen (20 μM) or ± mitoTEMPO (50 μM), using SiHa-F3 (J), B16-M4b (K), and SiHa-ρ0 (L) cells and WT counterparts.

All data represent means ± SEM. *$p < 0.05$, **$p < 0.01$, ***$p < 0.005$, ns, not significant versus untreated WT cells; $^{\#}p < 0.05$, $^{\#\#}p < 0.01$, $^{\#\#\#}p < 0.005$ versus the same treatment/cell type but without antioxidant, by Student's t test (G; J–L, left graphs) or one-way ANOVA (A–F, H, I; J–L, right graphs). See also Figure S2.

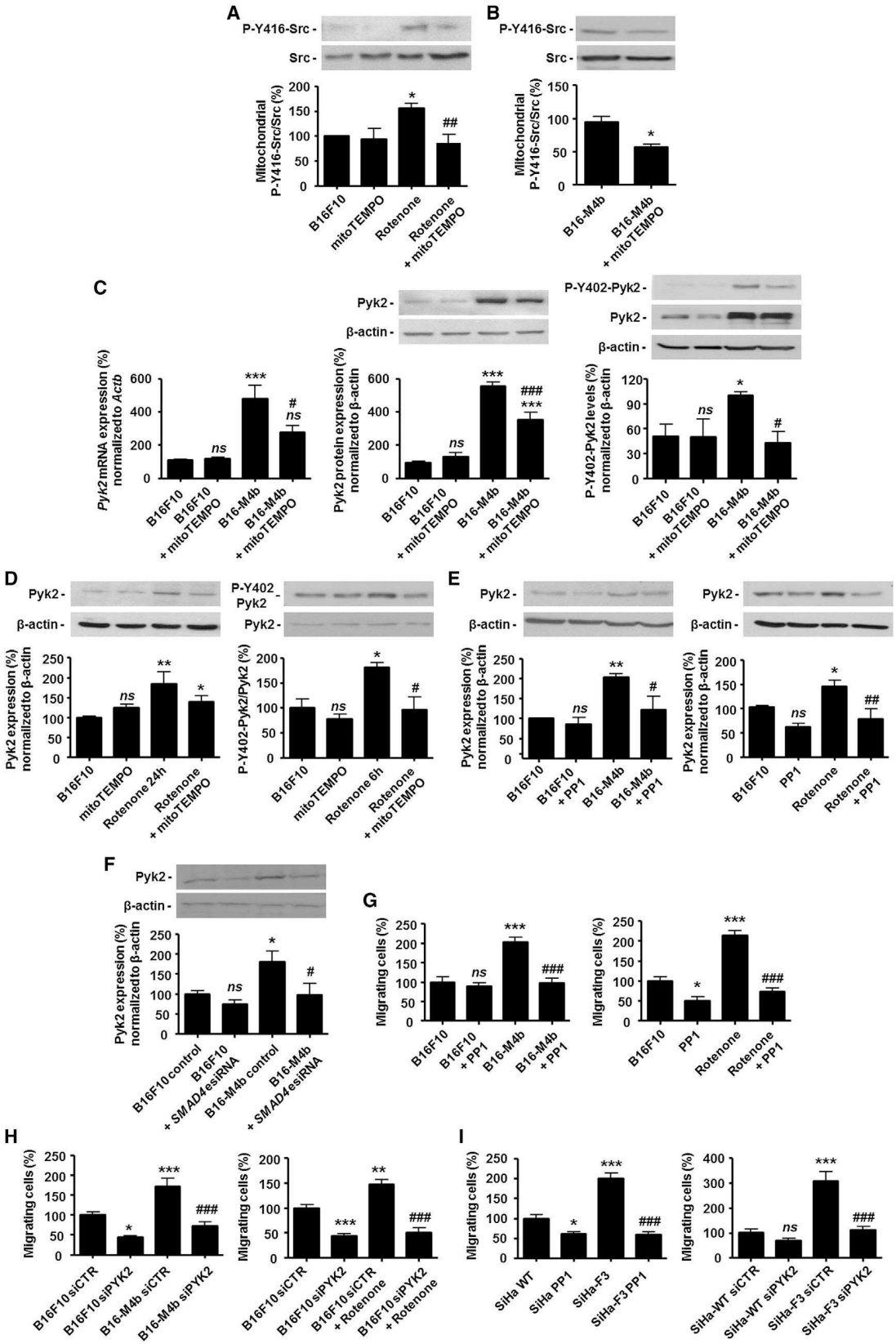

(legend on next page)

DISCUSSION

This study aimed to determine whether tumor cells performing aerobic glycolysis, the Warburg phenotype, are metastatic progenitors. The selection of superinvasive and supermetastatic tumor cells revealed a different phenotype that corresponds to a dysfunction of the TCA cycle associated with increased succinate and mitochondrial superoxide production. Mitochondrial ATP production was preserved. Metastasis was also enhanced upon partial ETC inhibition, another mitochondrial phenotype that shares with natural selection the capacity to induce mitochondrial superoxide production. Based on these findings, we document that spontaneous metastasis can be prevented with the mitochondria-targeted superoxide scavenger mitoTEMPO, with no overt toxicity.

Ishikawa et al. (2008a) previously showed that mtDNA mutations can trigger tumor metastasis. The prometastatic mitochondrial phenotype that we identified is different. Selection followed by biochemical characterization indeed revealed that superinvasive (Figure 1) and supermetastatic (Figure 2) tumor cells have undergone a common mitochondrial switch characterized by increased succinate production with or without increased glucose uptake and oxygen consumption, respectively. Supermetastatic cells displayed unaltered mitochondrial ATP production and no glycolytic compensation, thus ruling out the selection of OXPHOS-inactivating mutations. Therefore, increased succinate levels can be explained either by an overload of the TCA cycle (which is supported by the acquisition of large mitochondria with numerous cristae; Figure 2H), or by a dysfunction of the TCA cycle downstream of succinate dehydrogenase. When TCA cycle activity cannot be matched by ETC activity, mtROS production increases (Wellen and Thompson, 2010). Accordingly, we evidenced an increased mitochondrial superoxide production that can be linked in our models to increased production of electron donors, among which succinate can transfer electrons to succinate dehydrogenase at ETC complex II (Dröse and Brandt, 2012). Together, these observations indicate that the mitochondrial switch that we identified depends on ETC loading with excess electrons from the TCA cycle, without uncoupling the ETC from ATP synthase. Contrary to aerobic glycolysis, it did not provide a proliferative advantage (Figure S1B).

Conversely, moderate ETC inhibition can also promote tumor metastasis. Ishikawa et al. (2008b) indeed showed that the transfer of mitochondria with mtDNA mutations causing ETC complex I dysfunction increased the metastatic activity of weakly metastatic Lewis lung carcinoma cells (but it did not elicit de novo metastasis with nontransformed NIH 3T3 cells). Similar to ETC overloading, the prometastatic mitochondrial phenotype identified by these authors depends on increased mtROS production. Here, we went markedly beyond this previous finding by showing that partial inhibition (i.e., bottlenecking) of ETC complexes I to IV conferred a ROS-mediated prometastatic phenotype: whereas partial ETC inhibition improved tumor cell migration with all the strategies that we tested, the use of specific antioxidants and full ETC inhibition decreased migration (Figures 3A–3F). These data support the tenets of a hormetic window for mitochondrial ROS where moderate increase promotes tumorigenesis, whereas mtROS production above prometastatic levels would cause cell death (Sena and Chandel, 2012; Weinberg et al., 2010).

Excessive and deficient ETC activities generated the same superoxide-dependent prometastatic phenotype, which suggested the possibility of a common downstream mechanism. ROS in general and mtROS in particular are well known to contribute to tumor growth (Cannito et al., 2010; Dewhirst, 2009; Ferraro et al., 2006; Finley et al., 2011; Gao et al., 2007; Ishikawa et al., 2008a, 2008b; Miura et al., 2004; Nazarewicz et al., 2013a; Weinberg et al., 2010). Mitochondrial superoxide originates from electron leak at ETC complexes I and III (Muller et al., 2004). There, excess electrons are transferred to O_2 to form superoxide and, downstream, H_2O_2 (Wellen and Thompson, 2010). Using the antioxidants NAC and Ebselen, we showed H_2O_2 to be a pivotal promigratory effector of both metabotypes (Figure 3). Downstream of mtROS, both ETC dysfunctions further shared the ability to stimulate Src-Pyk2 signaling (Figures 4, S3, S4C, S4D, S5A, and S5B). Interestingly, Src activation occurred in the mitochondrial fraction of the cells (Figures 4A and 4B) and was unchanged in whole-cell lysates (not shown), highlighting it as a most upstream signaling event. Further downstream, Src induced the expression of Pyk2, a FAK family member protein tyrosine kinase that was previously reported to promote cytoskeletal remodeling and the migration, survival and epithelial-to-mesenchymal transition (EMT) of adherent cells (Gelman, 2003; Wendt et al., 2013). Unlike FAK, which is ubiquitously expressed, Pyk2 expression is induced by chemokines, TGF-β signaling, and following activation of G-protein-coupled receptors (Wendt et al., 2013). Our work indicates that mtROS can be included among pathophysiological inducers, with mitochondrial superoxide increasing Src-dependent, SMAD-induced Pyk2 transcription (Figure 4F), and activation (Figure 4), in agreement with previous reports indicating that ROS can activate Src, and showing that Pyk2 acts

Figure 4. A Src-SMAD-Pyk2 Pathway Accounts for mtROS-Induced Tumor Cell Migration

Where indicated, cells were treated with 10 nM rotenone, 50 μM mitoTEMPO or 10 μM of Src inhibitor PP1.

(A) Phospho-Y416-Src in the mitochondrial fraction of B16F10 cells (6 hr, n ≥ 3).

(B) As in (A) but using supermetastatic B16-M4b cells (n ≥ 3).

(C) *Pyk2* mRNA (left, 24 hr, n ≥ 5) and Pyk2 (middle, 24 hr, n ≥ 5) and phospho-Y402-Pyk2 (right, 6 hr, n ≥ 3) protein expression in B16F10 and B16-M4b cells.

(D) Pyk2 (left, n ≥ 5) and phospho-Y402-Pyk2 (right, n ≥ 3) protein expression in B16F10 cells (24 hr, n ≥ 3).

(E) Pyk2 protein expression in B16F10 and B16-M4b (left) and in B16F10 cells (right, 24 hr, n ≥ 3).

(F) Pyk2 protein expression in B16F10 and B16-M4b 48 hr after transfection with a control esiRNA (control) or a *SMAD4*-specific esiRNA (n = 3).

(G–I) Overnight migration. (G) Same cells and treatments as in (E) (n ≥ 3). (H) WT B16F10 versus supermetastatic B16-M4b cells (left); B16F10 cells (right). Cells expressed control SMARTpool siRNAs (siCTR) or SMARTpool siRNAs against Pyk2 (siPYK2, n ≥ 5 all). (I) SiHa-WT versus superinvasive SiHa-F3. Cells treated ± PP1 (left) or with control siRNA (siCTR) or a siRNA against *Pyk2* (right, n ≥ 4 all).

All data represent means ± SEM. *p < 0.05, **p < 0.01, ***p < 0.005, ns, not significant versus untreated/WT cells; $^{\#}$p < 0.05, $^{\#\#}$p < 0.01, $^{\#\#\#}$p < 0.005 versus the same treatment/cell type but without antioxidant or PP1, by one-way ANOVA (A, C–I) or by Student's t test (B). See also Table S1 and Figure S3.

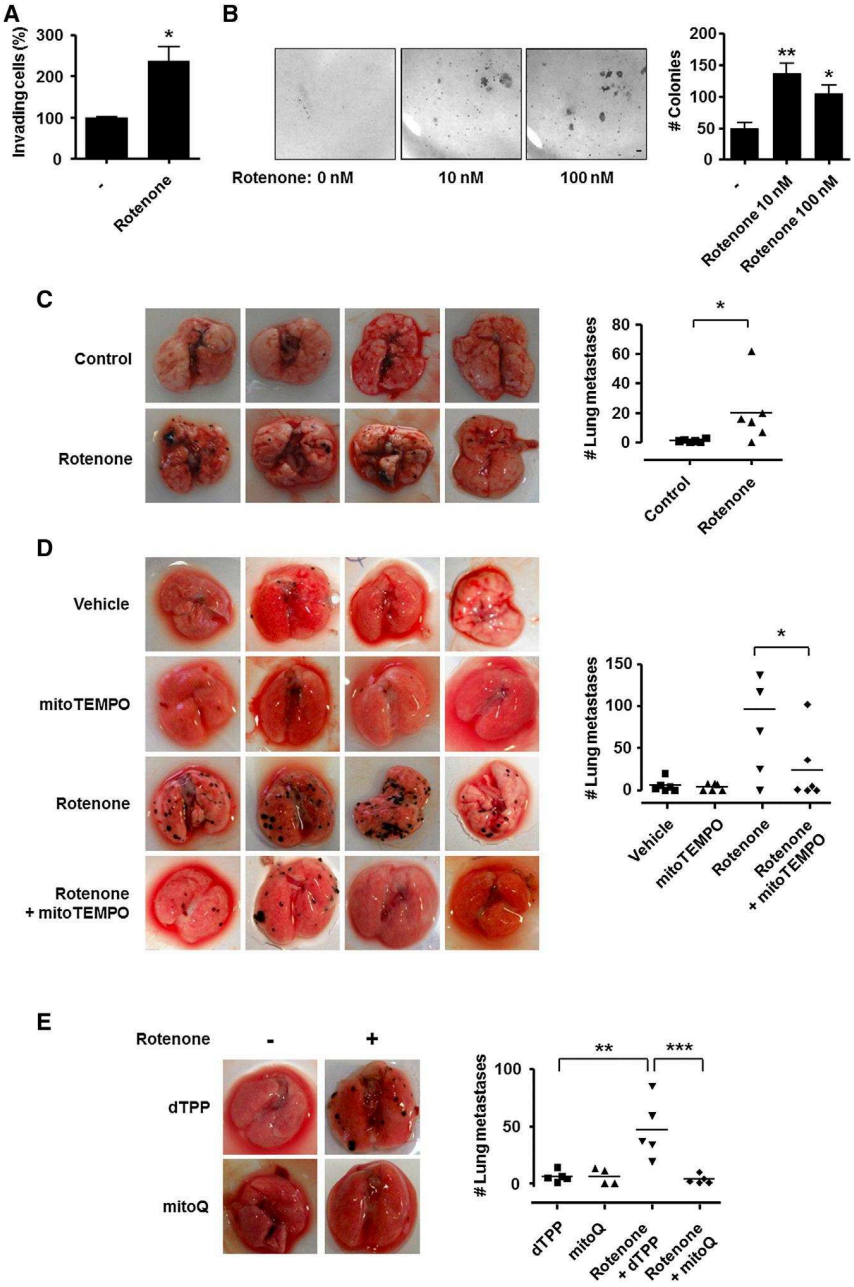

Figure 5. Mitochondrial ROS Scavenging Prevents Metastatic Take

(A–E) B16F10 tumor cells were treated with rotenone where indicated.

(A) Invasion assay (rotenone 10 nM, n = 3).

(B) Clonogenic assays (n ≥ 3) with cells pretreated for 6 hr with the indicated doses of rotenone.

(C) Experimental metastasis assay with B16F10 tumor cells constitutively expressing luciferase (B16F10-LUC) treated for 6 hr with 20 nM of rotenone or vehicle before tail vein injection. Mice were sacrificed 15 days later. Representative pictures of the lungs are shown and the number of lung metastases is quantified in the graph (n = 6).

(D) Determination of the number of lung metastases in syngeneic mice 15 days after the tail vein injection of B16F10 tumor cells treated with 20 nM rotenone and/or 50 μM of the mitochondria-selective superoxide-specific scavenger mitoTEMPO. Representative pictures of the lungs are shown and the number of lung metastases is quantified in the graph (n ≥ 5).

(E) As in (D) but using 1 μM of the mitochondria-targeted antioxidant mitoQ or dTPP (n = 4–5).

All data represent means ± SEM. *p < 0.05, **p < 0.01, ***p < 0.005, by Student's t test (A), one-way ANOVA (B, D, and E), or Mann-Whitney (C). See also Figure S4.

downstream of both ROS and Src (Andreev et al., 2001; Chiarugi et al., 2003; Gelman, 2003; Graham et al., 2012; Lluis et al., 2007; Wendt et al., 2013). Overall, Pyk2 is evidenced to be a main mediator of mitochondrial superoxide signaling, because its specific inhibition with si/shRNAs recapitulated the antimigratory and antimetastatic effects of mitoTEMPO (Figures 4G–4I and S4D–S4F). Our microarray data nevertheless suggest that additional effectors are likely to be involved.

We exploited the rationale provided by our in vitro findings to evaluate mtROS scavengers, targeting the most upstream mitochondrial event that was identified, in metastasis prevention. In different human and mouse models, the metastatic phenotype as a whole was lost when tumor-bearing mice were treated with the superoxide scavenger mitoTEMPO that we preferred to other common antioxidants for its high tropism for mitochondria (TPP group) and for its demonstrated specificity for superoxide (Dikalova et al., 2010; Nazarewicz et al., 2013a; Zhou et al., 2011). In particular, we report that mitoTEMPO prevents spontaneous metastasis of naturally metastatic MDA-MB-231 human breast cancer cells implanted orthotopically in the mouse mammary fat pad (Figure 6G). Many anticancer therapies rely on ROS-induced apoptosis. Although generic antioxidant effects on tumor growth are still debated (Gao et al., 2007; Sayin et al., 2014), mitoTEMPO compared to less selective antioxidants preserves physiological ROS signaling (as shown in nonmalignant fibroblasts; Nazarewicz et al., 2013a) and could therefore selectively target tumor cells with abnormal mitochondrial activities. Although we did not find significant primary tumor growth inhibition using mitoTEMPO at 0.7 mg/kg/day (Figure S5E), others (Nazarewicz et al., 2013a) have shown that the therapeutic effects of this drug at higher dose may retard primary tumor growth. MitoTEMPO acts as a SOD2 mimetic (Dikalova et al., 2010), raising the question of its impact on mitochondrial ROS detoxification, because it would promote H_2O_2 formation. In fact, by decreasing mitochondrial superoxide levels, mitoTEMPO impairs the

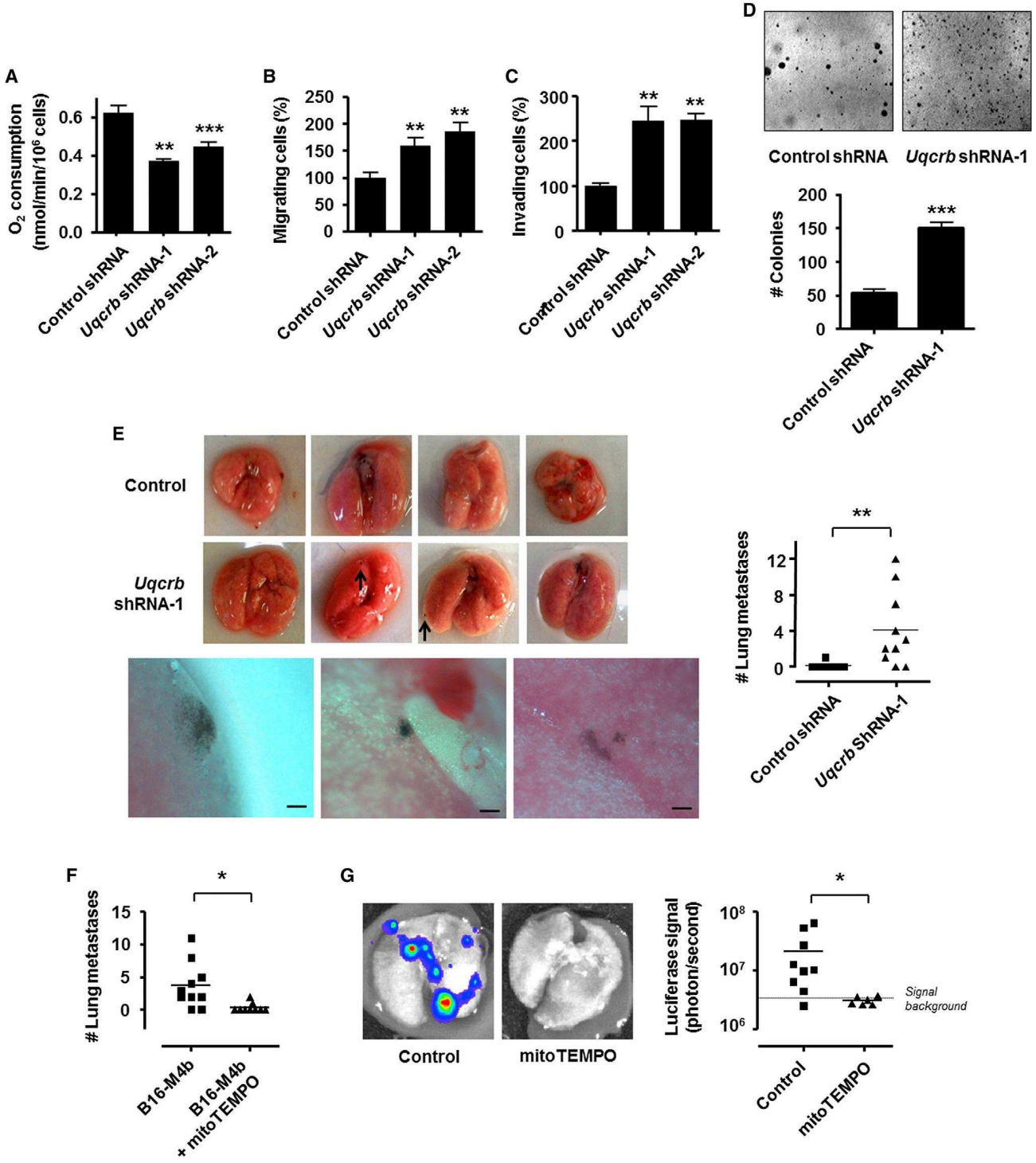

Figure 6. Mitochondrial ROS Scavenging Prevents Metastatic Tumor Dissemination

(A–E) B16F10 tumor cells were expressing specific shRNAs against complex III subunit *ubiquinol-cytochrome c reductase binding protein* (shUqcrb-1 or shUqcrb-2) or a control shRNA.

(A) Rotenone-sensitive oxygen consumption ($n \geq 3$).

(B) Overnight migration ($n \geq 11$).

(C) Overnight invasion ($n \geq 3$).

(D) Clonogenicity ($n = 6$).

(legend continued on next page)

formation of many different ROS derived from O_2, including cytosolic H_2O_2 (Nazarewicz et al., 2013b; Rogers et al., 2014) and self-propagating lipid peroxides (Mylonas and Kouretas, 1999), supporting efficient ROS detoxification. Similar to mitoTEMPO, mitoQ, a mitochondria-targeted form of coenzyme Q10 currently tested in clinical trials for applications other than cancer (Jin et al., 2013), blocked metastatic take (Figure 5). Collectively, these findings offer a rationale to test mitochondria-targeted superoxide scavengers, including mitoQ, in metastasis prevention trials.

In conclusion, we identified that aberrant TCA cycling coupled to mitochondrial superoxide production promotes tumor cell migration and metastasis. It represents a naturally selected, evolutionary alternative to ETC defects that also promote superoxide-dependent metastasis. Thus, tumor cells with increased mitochondrial superoxide production constitute a population of metastatic progenitors, and mitochondrial superoxide scavenging can be proposed as a therapeutic option to prevent spontaneous human tumor metastasis.

EXPERIMENTAL PROCEDURES

Animal Ethics Statement

All in vivo experiments were conducted under approval of the Université catholique de Louvain (UCL) authorities (Comité d'Ethique Facultaire pour l'Expérimentation Animale) according to national animal care regulations. Specific approval ID for this study was TUMETABO.

Cell Lines and Reagents

All assays were performed in DMEM with 4.5 g/l glucose without glutamine, pyruvate, and serum unless stated otherwise. SiHa human cervix squamous cell carcinoma and B16F1 and B16F10 murine melanoma tumor cells were purchased from ATCC, MDA-MB-231-LUC-D3H2LN human breast cancer cells and B16F10-LUC cells expressing firefly luciferase were from Caliper, and murine breast cancer cells 4T1 were a kind gift from Prof. Fred R. Miller (Karmanos Cancer Institute, Detroit, MI). These cells were routinely grown in DMEM containing glutamax and 4.5 g/l glucose supplemented with 10% fetal bovine serum (Gibco) and penicillin-streptomycin (Sigma-Aldrich) in a humidified atmosphere with 5% CO_2 at 37°C. For the generation of mitochondria-defective ρ0 cells, SiHa cells were treated with low-dose ethidium bromide (50 ng/ml) for 7 weeks and grown as previously described (Desjardins et al., 1986). SiHa-ρ0-D2 is a clonal cell line obtained by the limiting dilution of SiHa-ρ0. MitoTEMPO was from Santa-Cruz, PP1 and the Pyk2 inhibitor PF431396 from Abcam. MitoQ, and decyl-TPP were kind gifts of Prof. Michael P. Murphy. All other reagents were from Sigma-Aldrich and were dissolved in a DMSO vehicle.

Selection of Superinvasive and Supermetastatic Tumor Cells

Superinvasive SiHa-F3 cells were selected following three rounds of in vitro selection in BD BioCoat transwells (see Figure 1A). Supermetastatic B16-Mxy (where x represents the selection round and y independent selection identification) tumor cells were obtained by rounds of in vivo selection starting from WT B16F10 (see Figure 2A).

Functional Assays In Vitro

Cell migration and invasion were assayed in transwells, clonogenicity on soft agar, and proliferation with bromodeoxyuridine.

Metabolic Measurements

To avoid differences due to unequal growth rates, all measurements were made starting with confluent cells. All data were normalized by cell numbers. Oximetry was performed on a Seahorse XF96 bioenergetic analyzer and with electron paramagnetic resonance (EPR, Figure 6A). All data show mitochondrial oxygen consumption. The dose-dependent effect of rotenone on oxygen consumption was determined using MitoXpress (Luxcel Biosciences). All metabolic assays used enzymatic reactions with cells incubated for 24 hr in DMEM without glutamine, pyruvate, and serum.

Electron Microscopy

Transmission electron microscopy was performed using a previously described protocol (Piret et al., 2012).

ROS Measurements

MitoSOX was used to measure superoxide levels but has limited sensitivity and may not be fully selective for superoxide (Zielonka and Kalyanaraman, 2010). For this reason, ROS levels were measured with CM-H_2DCFDA, and the specific contribution of mtROS was verified in functional assays with specific inhibitors.

Cell Transfection, Quantitative RT-PCR, Immunoblotting, and Microarrays

Cell transfection with RNAi/MAX (Invitrogen) and infection with a third-generation lentiviral system are detailed in Supplemental Experimental Procedures. Quantitative RT-PCR and immunoblotting used previously disclosed protocols (Bouzin et al., 2007; Chianale et al., 2010). Following RNA isolation, whole-genome expression analysis was performed at Arraystar.

Metastatic Take and Spontaneous Metastasis Assays

For metastatic take assays, tumor cells were pretreated for 6 hr with the indicated drugs, and 10^6 viable cells were injected into the tail vein of syngeneic mice. For spontaneous metastasis assays, tumor cells were injected orthotopically to syngeneic or SCID mice to form primary tumors that were surgically removed when reaching a diameter of approximately 1 cm. Mice were treated daily with mitoTEMPO (0.7 mg/kg) or vehicle.

Statistics

All data are presented as means ± SEM. Student's t test, Mann-Whitney test and one-way ANOVA (Bonferroni post hoc test) were used where appropriate. $p < 0.05$ was considered statistically significant.

ACCESSION NUMBERS

Microarray data are available in the ArrayExpress database (http://www.ebi.ac.uk/arrayexpress) under accession number E-MTAB-2656.

SUPPLEMENTAL INFORMATION

Supplemental Information includes Supplemental Experimental Procedures, five figures, and one table and can be found with this article online at http://dx.doi.org/10.1016/j.celrep.2014.06.043.

AUTHOR CONTRIBUTIONS

P.S. supervised the project. P.E.P. and P.S. conceived experiments. P.E.P., V.L.P., J.P.-E., C.J.D., P.D., T.C., S.D., M.T., T.V., C.B., and C.M. performed and optimized experiments. P.E.P, V.L.P., J.P.-E., C.J.D., P.D., T.C., S.D.,

(E) Spontaneous metastasis assay: lung metastases were counted under a stereoscopic microscope 30 days after primary tumor implantation. Representative pictures of the lungs are shown (including at 5× magnification; scale bars, 200 μm), and the number of lung metastases is quantified in the graph ($n \geq 9$).
(F and G) Daily i.p. injections of mitoTEMPO (0.7 mg/kg) prevented spontaneous metastasis from primary orthotopic tumors generated with (F) supermetastatic B16-M4b cells (metastases counted under a stereoscopic microscope, $n \geq 9$), and (G) human breast cancer MDA-MB-231-LUC-D3H2LN cells (metastasis quantified using bioluminescence, $n \geq 6$).
All data represent means ± SEM. *$p < 0.05$, **$p < 0.01$, ***$p < 0.005$, by one-way ANOVA (A–C), Student's t test (D), or Mann-Whitney (E–G). See also Figure S5.

M.T., T.V., C.B., C.M., and P.S. analyzed and interpreted the data. O.F., C.M., B.G., and P.S. contributed to funding and expertise. P.E.P. and P.S. wrote the manuscript.

ACKNOWLEDGMENTS

This work was supported by the European Research Council (FP7/2007-2013 ERC Independent Researcher Starting Grant 243188 TUMETABO to P.S.), Interuniversity Attraction Pole (IAP) grant #UP7-03 from the Belgian Science Policy Office (Belspo), an Action de Recherche Concertée from the Communauté Française de Belgique (ARC 09/14-020), the Belgian Fondation contre le Cancer, the Belgian Fonds National de la Recherche Scientifique (F.R.S.-FNRS), the Fonds Joseph Maisin, and the UCL Fonds Spéciaux de la Recherche (FSR). O.F. is a honorary Research Director, P.S. a Research Associate, P.E.P. and P.D. Postdoctoral Researchers, and V.L.P. a Research Fellow of the F.R.S.-FNRS. C.J.D. is a Télévie Research Fellow. We thank Prof. Fred R. Miller (Karmanos Cancer Institute, Detroit, MI) for the kind gift of 4T1 cells; Prof. Michael P. Murphy (University of Cambridge, UK) for the kind gift of MitoQ and dTPP; Kirsten Dumaz and Julie De Wever (Keyrus Biopharma, Belgium) for professional English editing; Bjorn Baselet for scientific and technical input; the morphology platform and the electron microscopy service of the University of Namur; and Fabien Rodriguez, Floriane Ribeiro, and Marie-Joséphine Fontenille for excellent technical assistance. In memory of Mrs. Anne-Sophie Brouckaert, PharmD.

Received: April 26, 2013
Revised: June 4, 2014
Accepted: June 21, 2014
Published: July 24, 2014

REFERENCES

Anastasiou, D., Poulogiannis, G., Asara, J.M., Boxer, M.B., Jiang, J.K., Shen, M., Bellinger, G., Sasaki, A.T., Locasale, J.W., Auld, D.S., et al. (2011). Inhibition of pyruvate kinase M2 by reactive oxygen species contributes to cellular antioxidant responses. Science *334*, 1278–1283.

Andreev, J., Galisteo, M.L., Kranenburg, O., Logan, S.K., Chiu, E.S., Okigaki, M., Cary, L.A., Moolenaar, W.H., and Schlessinger, J. (2001). Src and Pyk2 mediate G-protein-coupled receptor activation of epidermal growth factor receptor (EGFR) but are not required for coupling to the mitogen-activated protein (MAP) kinase signaling cascade. J. Biol. Chem. *276*, 20130–20135.

Bouzin, C., Brouet, A., De Vriese, J., Dewever, J., and Feron, O. (2007). Effects of vascular endothelial growth factor on the lymphocyte-endothelium interactions: identification of caveolin-1 and nitric oxide as control points of endothelial cell anergy. J. Immunol. *178*, 1505–1511.

Brandon, M., Baldi, P., and Wallace, D.C. (2006). Mitochondrial mutations in cancer. Oncogene *25*, 4647–4662.

Brown, S.T., and Nurse, C.A. (2008). Induction of HIF-2alpha is dependent on mitochondrial O2 consumption in an O2-sensitive adrenomedullary chromaffin cell line. Am. J. Physiol. Cell Physiol. *294*, C1305–C1312.

Brown, L.M., Welch, D.R., and Rannels, S.R. (2002). B16F10 melanoma cell colonization of mouse lung is enhanced by partial pneumonectomy. Clin. Exp. Metastasis *19*, 369–376.

Cannito, S., Novo, E., di Bonzo, L.V., Busletta, C., Colombatto, S., and Parola, M. (2010). Epithelial-mesenchymal transition: from molecular mechanisms, redox regulation to implications in human health and disease. Antioxid. Redox Signal. *12*, 1383–1430.

Chang, Y.S., di Tomaso, E., McDonald, D.M., Jones, R., Jain, R.K., and Munn, L.L. (2000). Mosaic blood vessels in tumors: frequency of cancer cells in contact with flowing blood. Proc. Natl. Acad. Sci. USA *97*, 14608–14613.

Cheng, J.J., Chao, Y.J., and Wang, D.L. (2002). Cyclic strain activates redox-sensitive proline-rich tyrosine kinase 2 (PYK2) in endothelial cells. J. Biol. Chem. *277*, 48152–48157.

Chianale, F., Rainero, E., Cianflone, C., Bettio, V., Pighini, A., Porporato, P.E., Filigheddu, N., Serini, G., Sinigaglia, F., Baldanzi, G., and Graziani, A. (2010). Diacylglycerol kinase alpha mediates HGF-induced Rac activation and membrane ruffling by regulating atypical PKC and RhoGDI. Proc. Natl. Acad. Sci. USA *107*, 4182–4187.

Chiarugi, P., Pani, G., Giannoni, E., Taddei, L., Colavitti, R., Raugei, G., Symons, M., Borrello, S., Galeotti, T., and Ramponi, G. (2003). Reactive oxygen species as essential mediators of cell adhesion: the oxidative inhibition of a FAK tyrosine phosphatase is required for cell adhesion. J. Cell Biol. *161*, 933–944.

Desjardins, P., de Muys, J.M., and Morais, R. (1986). An established avian fibroblast cell line without mitochondrial DNA. Somat. Cell Mol. Genet. *12*, 133–139.

Dewhirst, M.W. (2009). Relationships between cycling hypoxia, HIF-1, angiogenesis and oxidative stress. Radiat. Res. *172*, 653–665.

Dikalova, A.E., Bikineyeva, A.T., Budzyn, K., Nazarewicz, R.R., McCann, L., Lewis, W., Harrison, D.G., and Dikalov, S.I. (2010). Therapeutic targeting of mitochondrial superoxide in hypertension. Circ. Res. *107*, 106–116.

Dong, M., Rice, L., Lepler, S., Pampo, C., and Siemann, D.W. (2010). Impact of the Src inhibitor saracatinib on the metastatic phenotype of a fibrosarcoma (KHT) tumor model. Anticancer Res. *30*, 4405–4413.

Dröse, S., and Brandt, U. (2012). Molecular mechanisms of superoxide production by the mitochondrial respiratory chain. Adv. Exp. Med. Biol. *748*, 145–169.

Faubert, B., Boily, G., Izreig, S., Griss, T., Samborska, B., Dong, Z., Dupuy, F., Chambers, C., Fuerth, B.J., Viollet, B., et al. (2013). AMPK is a negative regulator of the Warburg effect and suppresses tumor growth in vivo. Cell Metab. *17*, 113–124.

Ferraro, D., Corso, S., Fasano, E., Panieri, E., Santangelo, R., Borrello, S., Giordano, S., Pani, G., and Galeotti, T. (2006). Pro-metastatic signaling by c-Met through RAC-1 and reactive oxygen species (ROS). Oncogene *25*, 3689–3698.

Fidler, I.J. (1975). Biological behavior of malignant melanoma cells correlated to their survival in vivo. Cancer Res. *35*, 218–224.

Finley, L.W., Carracedo, A., Lee, J., Souza, A., Egia, A., Zhang, J., Teruya-Feldstein, J., Moreira, P.I., Cardoso, S.M., Clish, C.B., et al. (2011). SIRT3 opposes reprogramming of cancer cell metabolism through HIF1α destabilization. Cancer Cell *19*, 416–428.

Frezza, C., Pollard, P.J., and Gottlieb, E. (2011). Inborn and acquired metabolic defects in cancer. J. Mol. Med. *89*, 213–220.

Gambhir, S.S., Czernin, J., Schwimmer, J., Silverman, D.H., Coleman, R.E., and Phelps, M.E. (2001). A tabulated summary of the FDG PET literature. J. Nucl. Med. *42* (5, Suppl), 1S–93S.

Gao, P., Zhang, H., Dinavahi, R., Li, F., Xiang, Y., Raman, V., Bhujwalla, Z.M., Felsher, D.W., Cheng, L., Pevsner, J., et al. (2007). HIF-dependent antitumorigenic effect of antioxidants in vivo. Cancer Cell *12*, 230–238.

Gelman, I.H. (2003). Pyk 2 FAKs, any two FAKs. Cell Biol. Int. *27*, 507–510.

Graham, N.A., Tahmasian, M., Kohli, B., Komisopoulou, E., Zhu, M., Vivanco, I., Teitell, M.A., Wu, H., Ribas, A., Lo, R.S., et al. (2012). Glucose deprivation activates a metabolic and signaling amplification loop leading to cell death. Mol. Syst. Biol. *8*, 589.

Gupta, G.P., and Massagué, J. (2006). Cancer metastasis: building a framework. Cell *127*, 679–695.

Haut, S., Brivet, M., Touati, G., Rustin, P., Lebon, S., Garcia-Cazorla, A., Saudubray, J.M., Boutron, A., Legrand, A., and Slama, A. (2003). A deletion in the human QP-C gene causes a complex III deficiency resulting in hypoglycaemia and lactic acidosis. Hum. Genet. *113*, 118–122.

Ishikawa, K., Takenaga, K., Akimoto, M., Koshikawa, N., Yamaguchi, A., Imanishi, H., Nakada, K., Honma, Y., and Hayashi, J. (2008a). ROS-generating mitochondrial DNA mutations can regulate tumor cell metastasis. Science *320*, 661–664.

Ishikawa, K., Koshikawa, N., Takenaga, K., Nakada, K., and Hayashi, J. (2008b). Reversible regulation of metastasis by ROS-generating mtDNA mutations. Mitochondrion *8*, 339–344.

Jin, H., Kanthasamy, A., Ghosh, A., Anantharam, V., Kalyanaraman, B., and Kanthasamy, A.G. (2014). Mitochondria-targeted antioxidants for treatment of Parkinson's disease: Preclinical and clinical outcomes. Biochim. Biophys. Acta. *1842*, 1282–1294.

Kelso, G.F., Porteous, C.M., Coulter, C.V., Hughes, G., Porteous, W.K., Ledgerwood, E.C., Smith, R.A., and Murphy, M.P. (2001). Selective targeting of a redox-active ubiquinone to mitochondria within cells: antioxidant and antiapoptotic properties. J. Biol. Chem. *276*, 4588–4596.

Lluis, J.M., Buricchi, F., Chiarugi, P., Morales, A., and Fernandez-Checa, J.C. (2007). Dual role of mitochondrial reactive oxygen species in hypoxia signaling: activation of nuclear factor-kappaB via c-SRC and oxidant-dependent cell death. Cancer Res. *67*, 7368–7377.

Maciel, E.N., Kowaltowski, A.J., Schwalm, F.D., Rodrigues, J.M., Souza, D.O., Vercesi, A.E., Wajner, M., and Castilho, R.F. (2004). Mitochondrial permeability transition in neuronal damage promoted by Ca2+ and respiratory chain complex II inhibition. J. Neurochem. *90*, 1025–1035.

Miura, D., Miura, Y., and Yagasaki, K. (2004). Resveratrol inhibits hepatoma cell invasion by suppressing gene expression of hepatocyte growth factor via its reactive oxygen species-scavenging property. Clin. Exp. Metastasis *21*, 445–451.

Muller, F.L., Liu, Y., and Van Remmen, H. (2004). Complex III releases superoxide to both sides of the inner mitochondrial membrane. J. Biol. Chem. *279*, 49064–49073.

Mylonas, C., and Kouretas, D. (1999). Lipid peroxidation and tissue damage. In Vivo *13*, 295–309.

Nazarewicz, R.R., Dikalova, A., Bikineyeva, A., Ivanov, S., Kirilyuk, I.A., Grigor'ev, I.A., and Dikalov, S.I. (2013a). Does scavenging of mitochondrial superoxide attenuate cancer prosurvival signaling pathways? Antioxid. Redox Signal. *19*, 344–349.

Nazarewicz, R.R., Dikalova, A.E., Bikineyeva, A., and Dikalov, S.I. (2013b). Nox2 as a potential target of mitochondrial superoxide and its role in endothelial oxidative stress. Am. J. Physiol. Heart Circ. Physiol. *305*, H1131–H1140.

Nguyen, D.X., Bos, P.D., and Massagué, J. (2009). Metastasis: from dissemination to organ-specific colonization. Nat. Rev. Cancer *9*, 274–284.

Piret, J.P., Vankoningsloo, S., Mejia, J., Noël, F., Boilan, E., Lambinon, F., Zouboulis, C.C., Masereel, B., Lucas, S., Saout, C., and Toussaint, O. (2012). Differential toxicity of copper (II) oxide nanoparticles of similar hydrodynamic diameter on human differentiated intestinal Caco-2 cell monolayers is correlated in part to copper release and shape. Nanotoxicology *6*, 789–803.

Porporato, P.E., Dhup, S., Dadhich, R.K., Copetti, T., and Sonveaux, P. (2011). Anticancer targets in the glycolytic metabolism of tumors: a comprehensive review. Front. Pharmacol. *2*, 49.

Rogers, C., Davis, B., Neufer, P.D., Murphy, M.P., Anderson, E.J., and Robidoux, J. (2014). A transient increase in lipid peroxidation primes preadipocytes for delayed mitochondrial inner membrane permeabilization and ATP depletion during prolonged exposure to fatty acids. Free Radic. Biol. Med. *67*, 330–341.

Roussos, E.T., Condeelis, J.S., and Patsialou, A. (2011). Chemotaxis in cancer. Nat. Rev. Cancer *11*, 573–587.

Sayin, V.I., Ibrahim, M.X., Larsson, E., Nilsson, J.A., Lindahl, P., and Bergo, M.O. (2014). Antioxidants accelerate lung cancer progression in mice. Sci. Transl. Med. *6*, 221ra15.

Schewe, T. (1995). Molecular actions of ebselen—an antiinflammatory antioxidant. Gen. Pharmacol. *26*, 1153–1169.

Sena, L.A., and Chandel, N.S. (2012). Physiological roles of mitochondrial reactive oxygen species. Mol. Cell *48*, 158–167.

Sherer, T.B., Betarbet, R., Testa, C.M., Seo, B.B., Richardson, J.R., Kim, J.H., Miller, G.W., Yagi, T., Matsuno-Yagi, A., and Greenamyre, J.T. (2003). Mechanism of toxicity in rotenone models of Parkinson's disease. J. Neurosci. *23*, 10756–10764.

Sonveaux, P., Végran, F., Schroeder, T., Wergin, M.C., Verrax, J., Rabbani, Z.N., De Saedeleer, C.J., Kennedy, K.M., Diepart, C., Jordan, B.F., et al. (2008). Targeting lactate-fueled respiration selectively kills hypoxic tumor cells in mice. J. Clin. Invest. *118*, 3930–3942.

Tsukihara, T., Aoyama, H., Yamashita, E., Tomizaki, T., Yamaguchi, H., Shinzawa-Itoh, K., Nakashima, R., Yaono, R., and Yoshikawa, S. (1996). The whole structure of the 13-subunit oxidized cytochrome c oxidase at 2.8 A. Science *272*, 1136–1144.

Vander Heiden, M.G., Cantley, L.C., and Thompson, C.B. (2009). Understanding the Warburg effect: the metabolic requirements of cell proliferation. Science *324*, 1029–1033.

Vaupel, P., and Mayer, A. (2012). Availability, not respiratory capacity governs oxygen consumption of solid tumors. Int. J. Biochem. Cell Biol. *44*, 1477–1481.

Warburg, O. (1956). On the origin of cancer cells. Science *123*, 309–314.

Ward, P.S., and Thompson, C.B. (2012). Metabolic reprogramming: a cancer hallmark even warburg did not anticipate. Cancer Cell *21*, 297–308.

Weinberg, F., Hamanaka, R., Wheaton, W.W., Weinberg, S., Joseph, J., Lopez, M., Kalyanaraman, B., Mutlu, G.M., Budinger, G.R., and Chandel, N.S. (2010). Mitochondrial metabolism and ROS generation are essential for Kras-mediated tumorigenicity. Proc. Natl. Acad. Sci. USA *107*, 8788–8793.

Wellen, K.E., and Thompson, C.B. (2010). Cellular metabolic stress: considering how cells respond to nutrient excess. Mol. Cell *40*, 323–332.

Wendt, M.K., Schiemann, B.J., Parvani, J.G., Lee, Y.H., Kang, Y., and Schiemann, W.P. (2013). TGF-β stimulates Pyk2 expression as part of an epithelial-mesenchymal transition program required for metastatic outgrowth of breast cancer. Oncogene *32*, 2005–2015.

Zhou, R., Yazdi, A.S., Menu, P., and Tschopp, J. (2011). A role for mitochondria in NLRP3 inflammasome activation. Nature *469*, 221–225.

Zielonka, J., and Kalyanaraman, B. (2010). Hydroethidine- and MitoSOX-derived red fluorescence is not a reliable indicator of intracellular superoxide formation: another inconvenient truth. Free Radic. Biol. Med. *48*, 983–1001.

Metabolic metastasis

A mitochondrial switch promotes tumor metastasis

Paolo E. Porporato, Valéry L. Payen, Jhudit Pérez-Escuredo, Christophe J. De Saedeleer, Pierre Danhier, Tamara Copetti, Suveera Dhup, Morgane Tardy, Thibaut Vazeille, Caroline Bouzin, Olivier Feron, Carine Michiels, Bernard Gallez, and Pierre Sonveaux

---

SUPPLEMENTAL DATA

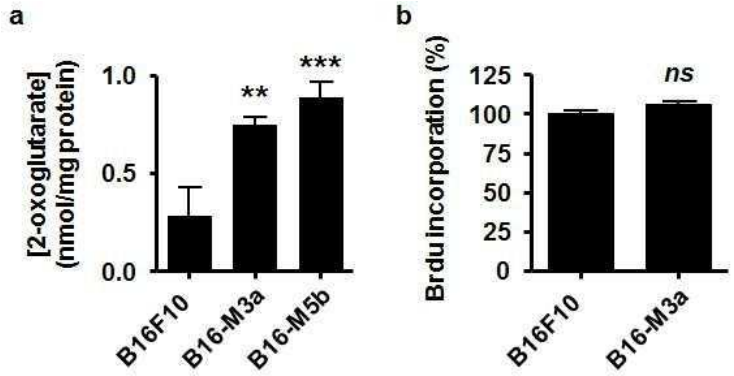

Figure S1. Compared to B16F10, supermetastatic B16-M3a/5b cells have increased intracellular 2-oxoglutarate levels but unchanged proliferation rate, related to Figure 2. (**A**) Intracellular 2-oxoglutarate levels ($n \geq 4$). (**B**) Proliferation rates quantified from BrdU incorporation ($n = 4$). Data represent means ± SEM. ** $P < 0.01$, *** $P < 0.005$, *ns* not significant compared to B16F10, by one-way ANOVA (**A**) or Student's *t* test (**B**).

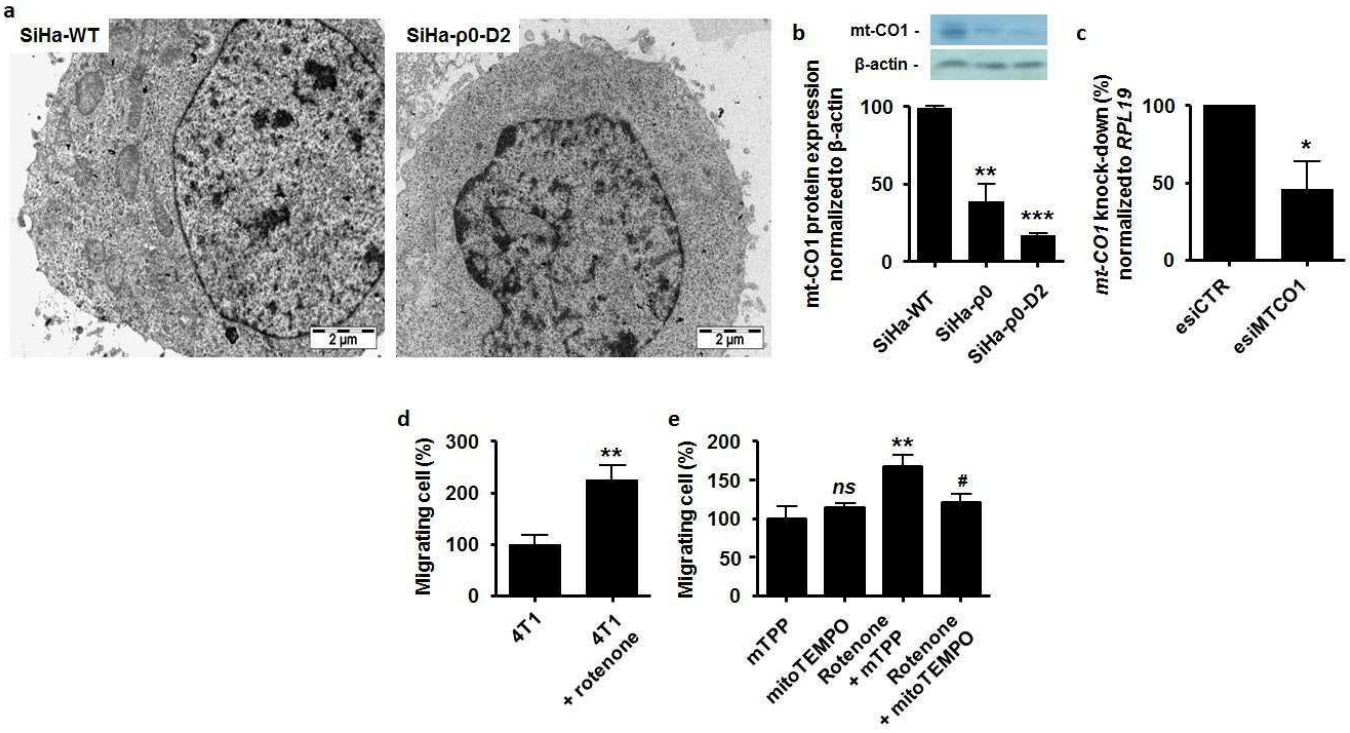

Figure S2. Validation of SiHa models, promotion by rotenone of 4T1 cell migration, and methyltriphenylphosphonium control of SiHa cell migration, related to Figure 3. (**A**) Representative electron microscopic pictures of SiHa-WT and SiHa-ρ0-D2 cells. (**B**) Western blot quantification of the mitochondria-encoded protein mt-CO1 in SiHa-WT, SiHa-ρ0 and SiHa-ρ0-D2 cells (n = 3). (**C**) Relative *mt-CO1* mRNA expression determined using RT-qPCR in SiHa cells transfected with a specific esiRNA (esiMTCO1) or a control esiRNA (esiCTR, n = 3). (**D**) Overnight migration of 4T1 cells treated with rotenone (10 nM) or not (n = 6). (**E**) Overnight migration assays of SiHa-WT tumor cells treated with methyltriphenylphosphonium (mTPP, 50 µM), mitoTEMPO (50 µM) and/or rotenone (10 nM) (n = 6). Data represent means ± SEM. * P < 0.05, ** P < 0.01, *** P < 0.005, *ns* not significant *versus* control (first column); $^{\#}$ P < 0.05 *versus* rotenone + mTPP; by one-way ANOVA (**B, E**) or Student's t test (**C, D**).

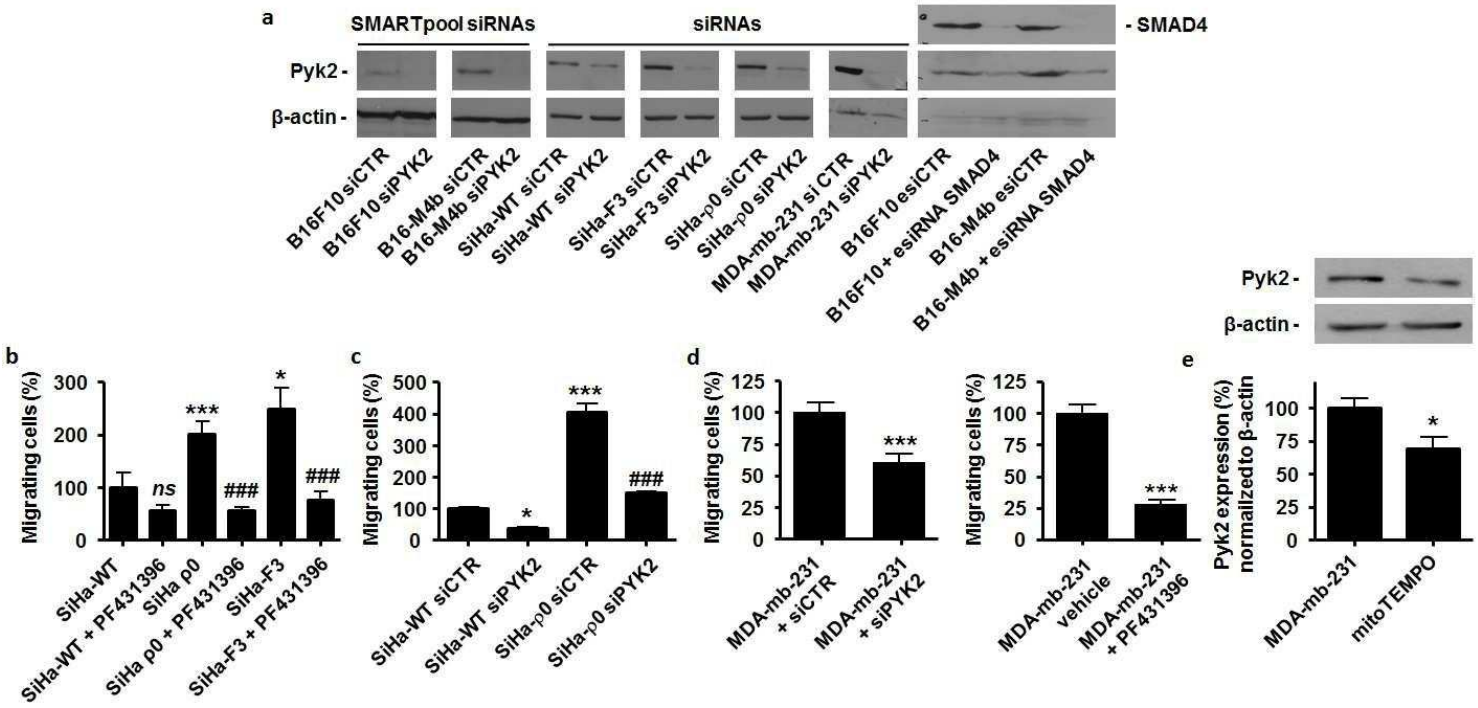

Figure S3. Confirmation that Pyk2 promotes mtROS-dependent tumor migration, related to Figure 4. (**A**) Representative immunoblots showing Pyk2, SMAD4 and β-actin expression in murine tumor cells transfected with control SMARTpool siRNAs (siCTR) or SMARTpool siRNAs against Pyk2 (siPYK2), human tumor cells transfected with a control siRNA (siCTR) or a specific siRNA targeting *Pyk2* (siPYK2), and murine cells transfected with a control esiRNA (esiCTR) or a specific esiRNA targeting *SMAD4*. (**B**) Overnight migration of wild-type SiHa (SiHa-WT), SiHa-F3 and SiHa-ρ0 tumor cells ± PF431396 (2.5 µM) (n = 6). (**C**) Overnight migration of SiHa-WT and SiHa-ρ0 tumor cells expressing siCTR or siPYK2 ($n \geq 4$) (**D**) Overnight migration of MDA-MB-231 human breast cancer cells expressing siCTR or siPYK2 (left panel) or treated ± PF431396 (2.5 µM) (right panel; $n \geq 6$). (**E**) Pyk2 protein expression in MDA-MB-231 cells ± 50 µM mitoTEMPO (24h treatment; n = 5). Data represent means ± SEM. * $P < 0.05$, *** $P < 0.005$, *ns* not significant *versus* control; $^{###}$ $P < 0.005$ *versus* same cells without PF431396 (**B**) or SiHa-ρ0 cells transfected with siCTR (**C**); by one-way ANOVA (**B, C**) or Student's t test (**D, E**)

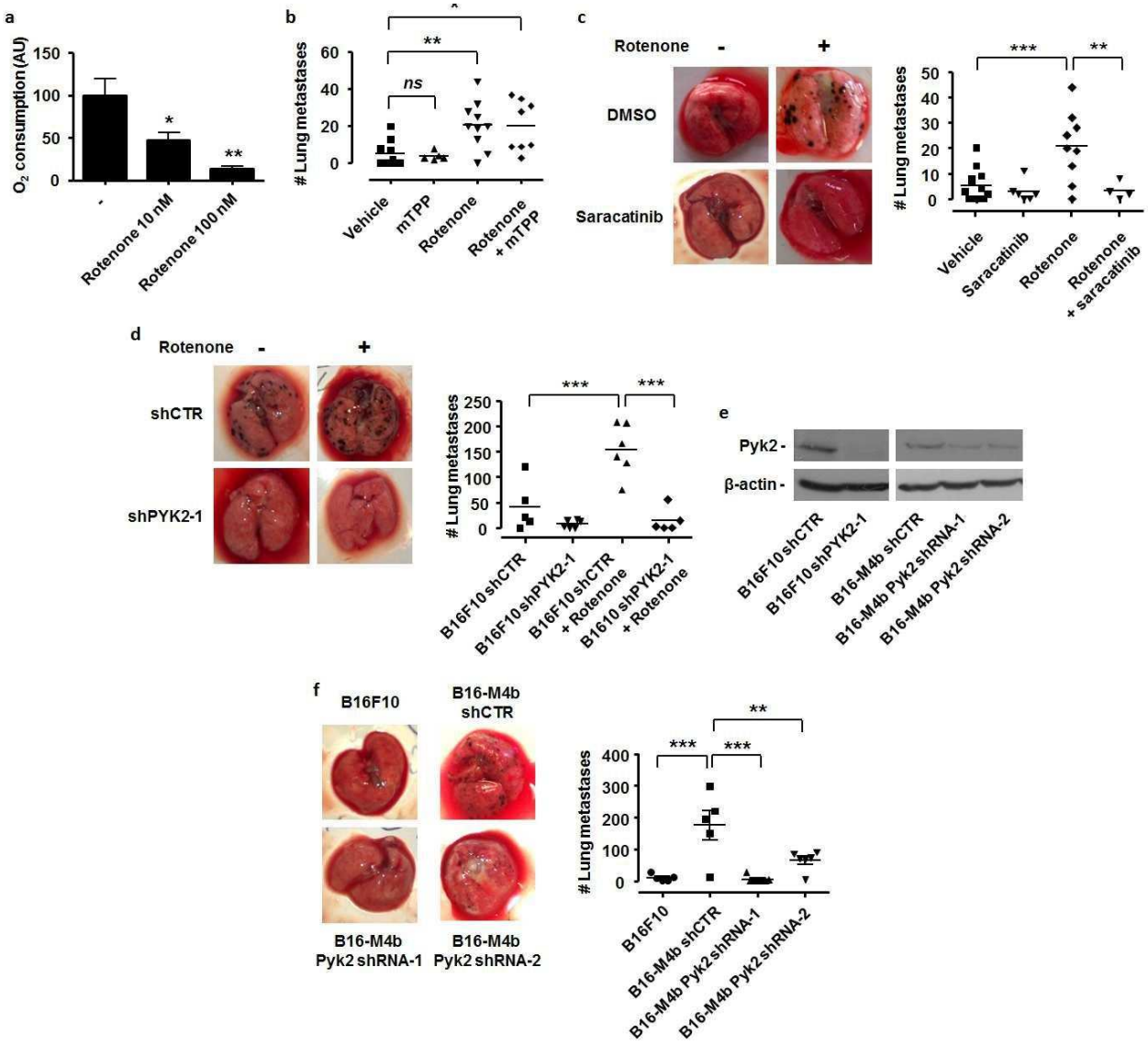

Figure S4. Confirmation of a metabolic control of metastatic take involving mtROS-Src-Pyk2 signaling, related to Figure 5. (**A**) Oxygen consumption was measured using MitoXpress in B16F10 cells treated with different concentrations of rotenone as indicated (n = 4). (**B**) Determination of the number of lung metastases in syngeneic mice 15 days after the tail vein injection of B16F10 tumor cells pretreated for 6h with 20 nM rotenone and/or 50 µM of methyltriphenylphosphonium (mTPP) ($n \geq 5$). (**C**) As in (D) but using the Src inhibitor Saracatinib (5 µM). Representative pictures of the lungs are also shown ($n \geq 4$). (**D**) B16F10 cells were infected with a control shRNA (shCTR) or a specific shRNA targeting *Pyk2* (shPYK2-1) were injected in the tail vein of syngeneic mice. Lung macrometastases were counted under a stereoscopic microscope 16 days after injection. Representative pictures of the lungs are shown and the number of lung metastases is quantified in the graph ($n \geq 5$) (**E**) Representative immunoblots showing Pyk2 and β-actin expression in B16F10 and B16-M4b cells transfected with shCTR, shPYK2-1 or shPYK2-2. (**F**) Experimental metastasis assay with B16-M4b expressing shCTR, shPYK2-1 or shPYK2-2, and B16F10 cells (control). Mice were sacrificed 15 days after tail vein injection. Representative pictures of the lungs are shown and the number of lung metastases is quantified in the graph ($n \geq 5$). Data represent means ± SEM. * $P < 0.05$, ** $P < 0.01$, *** $P < 0.005$, *ns* not significant by one-way ANOVA.

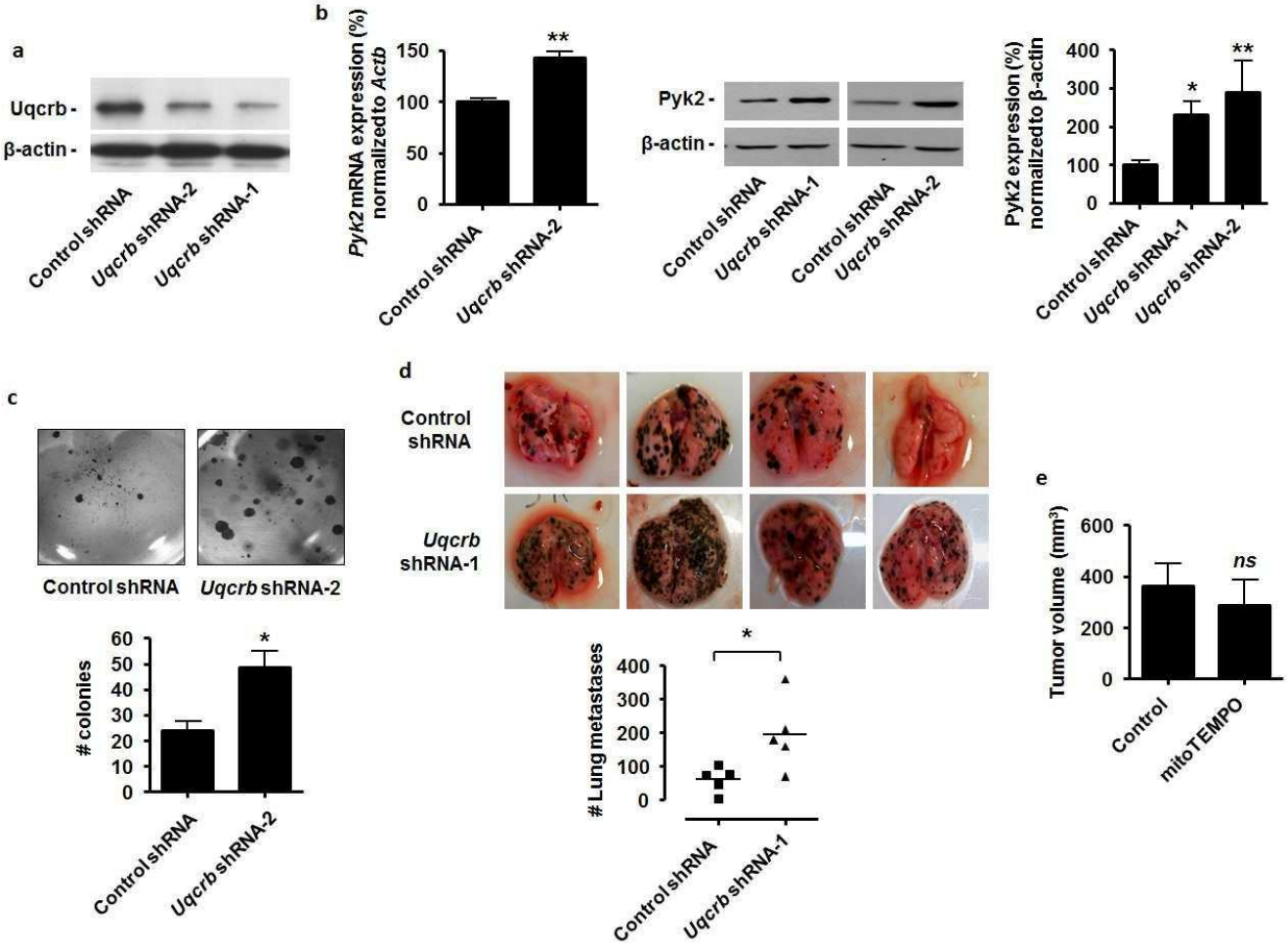

Figure S5. Partial inhibition of respiratory complex III promotes Pyk2 expression, clonogenicity and experimental metastasis, related to Figure 6. (**A**-**D**) B16F10 cells expressed a specific shRNA against complex III subunit *ubiquinol-cytochrome c reductase binding protein* (shUQCRB-1 or shUQCRB-2) or a control shRNA. (**A**) Immunoblot showing Uqcrb expression. (**B**) *Pyk2* mRNA (*left*, $n = 3$) and Pyk2 protein (*right*, $n \geq 3$) expression. (**C**) Clonogenicity on soft agar. ($n = 4$). (**D**) Determination of the number of lung metastases 15 days after the tail vein injection of cells to syngeneic mice (lung macrometastases were counted under a stereoscopic microscope, $n = 5$). (**D**) Tumor volume at Day +28 following the implantation of primary tumors established with MDA-MB-231-LUC-D3H2LN cells in SCID mice (same animals as in Figure 6G). From the day of primary tumor implantation, mice were daily injected with mitoTEMPO (0.7mg/Kg) or an equal amount of vehicle (control) ($n \geq 6$). Data represent means ± SEM. * $P < 0.05$, ** $P < 0.01$, *ns* not significant; by Student's *t* test (**B** *left*, **C**-**E**) or one-way ANOVA (**B** *right*).

Table S1. Genes sharing differential expression in rotenone-treated B16F10, B16-M2a and B16-M4b *versus* B16F10 mouse melanoma tumor cells, related to Figure 4.

Gene		Fold Change	Regulation	*P*
Symbol	**Name**			
Trp73	transformation related protein 73, transcript variant 1	1.63	up	0.0014
Setd3	SET domain containing 3	1.79	up	0.0020
Polh	polymerase (DNA directed), eta (RAD 30 related)	1.81	up	0.0055
Prdm9	PR domain containing 9	1.82	up	0.0099
Ptk2b	PTK2 protein tyrosine kinase 2 beta, transcript variant 2	1.51	up	0.0116
Kctd11	potassium channel tetramerisation domain containing 11	2.46	up	0.0137
Rhox10	reproductive homeobox 10	1.51	up	0.0146
Olfr170	olfactory receptor 170	1.61	up	0.0205
Msmb	β-microseminoprotein	1.94	up	0.0256
Ccdc85a	coiled-coil domain containing 85A, transcript variant 1	1.92	up	0.0266
Ush1c	Usher syndrome 1C homolog (human), transcript variant b4	3.82	up	0.0302
Vwf	Von Willebrand factor homolog	1.79	up	0.0322
Zdhhc23	hypothetical Zn-finger, DHHC type/Zinc finger DHHC-type profile containing protein	1.69	up	0.0354
Ddo	*D*-aspartate oxidase	1.57	up	0.0364
Cwc25	CWC25 spliceosome-associated protein homolog (S. cerevisiae)	1.69	up	0.0370
Svopl	SV2 related protein homolog (rat)-like	1.79	up	0.0372
Marveld3	MARVEL (membrane-associating) domain containing 3, transcript variant 1	2.17	up	0.0372
Lrfn1	leucine rich repeat and fibronectin type III domain containing 1, transcript variant 1	1.68	up	0.0373
Mpl	myeloproliferative leukemia virus oncogene, transcript variant 2	1.55	up	0.0388
Sct	secretin	1.93	up	0.0396
Cyp2b9	cytochrome P450, family 2, subfamily b, polypeptide 9	1.59	up	0.0406
Rph3a	rabphilin 3A	2.54	up	0.0409
Dhx37	DEAH (Asp-Glu-Ala-His) box polypeptide 37	1.72	up	0.0415
Ceacam16	carcinoembryonic antigen-related cell adhesion molecule 16	1.54	up	0.0440
Mrvi1	MRV integration site 1, transcript variant 2	1.78	up	0.0449
Adm2	adrenomedullin 2	1.61	up	0.0495
Cd300lb	CD300 antigen like family member B	3.75	up	0.0497
Krtap16-8	keratin associated protein 16-8	1.62	down	0.0169
	histone deacetylase 1 (Gallus gallus)	1.57	down	0.0418
Scgb3a2	secretoglobin, family 3A, member 2	1.72	down	0.0419
Cdh7	cadherin 7, type 2	1.93	down	0.0011
Hc	hemolytic complement (Hc)	1.62	down	0.0239
Vwc2	von Willebrand factor C domain containing 2	1.62	down	0.0442
	immunoglobulin kappa variable 4-57-1	1.62	down	0.0309
Lyzl1	lysozyme-like 1	1.90	down	0.0067
Mcpt8	mast cell protease 8	2.76	down	0.0010
Olfr1404	olfactory receptor 1404	1.54	down	0.0460

Metabolic metastasis

Ppp1r12b	protein phosphatase 1, regulatory (inhibitor) subunit 12B, transcript variant 1	1.59	down	0.0026
Mrc1	mannose receptor, C type 1	1.78	down	0.0027
Olfr50	olfactory receptor 50	3.43	down	0.0148
Krtap16-5	keratin associated protein 16-5	1.86	down	0.0299
	vomeronasal 2, receptor, pseudogene 106	3.72	down	0.0498
Cd70	CD70 antigen	3.31	down	0.0361
Kap	kidney androgen regulated protein	1.98	down	0.0329
Emid2	EMI domain containing 2	1.52	down	0.0420
Ccl26	chemokine (C-C motif) ligand 26	2.61	down	0.0477
Olfr1228	olfactory receptor 1228	2.47	down	0.0025
Olfr899	olfactory receptor 899	1.70	down	0.0198
Hbq1a	hemoglobin, theta 1A	2.37	down	0.0353
Bves	blood vessel epicardial substance	2.31	down	0.0055
Gabre	gamma-aminobutyric acid (GABA) A receptor, subunit epsilon	1.57	down	0.0386
Gucy1a3	guanylate cyclase 1, soluble, alpha 3	2.74	down	0.0234
Camk2a	calcium/calmodulin-dependent protein kinase II alpha	1.72	down	0.0420
Defb13	defensin beta 13	2.44	down	0.0076
Vmn2r-ps57	calcium-sensing receptor related sequence 1 (Casr-rs1)	3.21	down	0.0224
Ufm1	ubiquitin-fold modifier 1	2.92	down	0.0075
Ccr5	chemokine (C-C motif) receptor 5	2.62	down	0.0467
Mrpl21	mitochondrial ribosomal protein L21, nuclear gene encoding mitochondrial protein	1.54	down	0.0223
Olfr693	olfactory receptor 693	2.99	down	0.0285
Gal3st3	galactose-3-O-sulfotransferase 3	1.85	down	0.0082
Prss29	protease, serine, 29	1.95	down	0.0093
Pdia2	protein disulfide isomerase associated 2	1.77	down	0.0258
Lrit1	leucine-rich repeat, immunoglobulin-like and transmembrane domains 1	1.70	down	0.0240
Ace2	angiotensin I converting enzyme (peptidyl-dipeptidase A) 2 (Ace2)	1.68	down	0.0439
Olfr533	olfactory receptor 533	1.55	down	0.0380
Apol10b	apolipoprotein L 10b	1.78	down	0.0070
Sec1	secretory blood group 1	1.59	down	0.0046
Mdn1	midasin homolog (yeast)	1.50	down	0.0447
Gli1	GLI-Kruppel family member GLI1	2.52	down	0.0250
Tbx5	T-box 5	1.92	down	0.0080
Anxa4	annexin A4	2.06	down	0.0424
Csnk1g3	casein kinase 1, gamma 3	1.82	down	0.0269
Aldh1a7	aldehyde dehydrogenase family 1, subfamily A7	1.61	down	0.0267
Stk32a	serine/threonine kinase 32A (Stk32a)	1.59	down	0.0472
Trank1	tetratricopeptide repeat and ankyrin repeat containing 1	1.75	down	0.0130
Pla2g12b	phospholipase A2, group XIIB	1.79	down	0.0407

SUPPLEMENTAL EXPERIMENTAL PROCEDURES

Selection of superinvasive and supermetastatic tumor cells

Superinvasive SiHa-F3 cells were selected following three rounds of *in vitro* selection in BD BioCoat transwells. Briefly, following overnight invasion towards serum, cells in the bottom of the transwell were trypsinized and expanded in a separate dish.

Supermetastatic B16-Mxy (where x represents the selection round and y independent selection identification) tumor cells were obtained by rounds of *in vivo* selection starting from wild-type B16F10. Briefly, 10^6 B16F10 cells were injected subcutaneously to form a primary tumor in 8 week-old male C57BL/6j mice (Janvier). When the tumors reached a diameter of approximately 1 cm, primary tumors were carefully resected and removed in order to promote metastatic outgrowth (Gabri et al., 2006). Mice were sacrificed using ketamine/xylazine overdose followed by cervical dislocation 2 to 3 months after primary tumor removal. Lungs were necropsied and metastases were carefully isolated and cleaned of any conjunctive tissue under a stereoscopic microscope. Isolated cells were put in culture, expanded and re-injected subcutaneously to form a primary tumor in the next animals. Selection was performed twice in parallel starting from 2 different populations of B16F10 cells to yield B16-M2/3a (2 and 3 generations) and B16-M4/5b (4 and 5 generations) belonging to two independent cell lineages.

Cell migration and invasion

Migration/chemotaxis assays were performed in a NeuroProbe standard 48-well chemotaxis chamber according to manufacturer's instructions. Briefly, the bottom chamber was filled with DMEM without glutamine and pyruvate containing 0.1% serum as chemo-attractant. 50,000 cells were seeded in the upper chamber in the same medium but without serum, and allowed to migrate overnight through an 8-µm pore size polycarbonate membrane. Migrated cells were fixed and stained with Diff-Quick (Dade Behring) before counting. Invasion assays were performed in a 1% serum gradient using BD BioCoat Matrigel transwells, seeding 100,000 cells per well.

Clonogenicity

Clonogenicity on soft agar was performed as previously described (Filigheddu et al., 2007). Briefly, cells were suspended in 0.4% agar in full DMEM with 10% FCS and plated (1,000 cells/well, 12-well plates) on a layer of 0.8% agar in the same medium. Cells were incubated at 37 °C with 0.5 ml of medium. After 3 weeks, the colonies of living cells were determined after yellow MTT tetrazolium coloration, and counted using the ImageJ software (National Institutes of Health).

Proliferation

Proliferation was quantified using the BrdU Proliferation Kit ELISA colorimetric assay from Roche according to manufacturer's instructions. Briefly, 5,000 cells were plated in 96-well plates, serum-starved overnight, and stimulated with the indicated treatment for 24-h. BrdU was added in the last 16 hours of the experiments.

Oximetry

Oximetry on confluent cells was performed using a Seahorse XF96 bioenergetic analyzer with a mitostress kit (Seahorse Biosciences). Briefly, 20,000 cells/well were plated one day in advance according to manufacturer's protocol. Following the assay, cells were lysed with 0.5 M NaOH and quantified with BCA protein quantification (Thermo Scientific). Data were normalized for total protein content. Mitochondrial oxygen consumption was determined by paired measurements ± full ETC inhibition with rotenone and antimycin, following supplier's

instructions. In Figure 6A, oximetry was performed using electron paramagnetic resonance (EPR). EPR spectra were recorded on a Bruker EMX EPR spectrometer operating at 9.5 GHz. Cells were suspended in 10% dextran (to maintain cells in suspension) in DMEM. A neutral nitroxide, ^{15}N 4-oxo-2,2,6,6-tetramethylpiperidine-d_{16}-^{15}N-1-oxyl, at 0.2 mM (CDN Isotopes, Pointe-Claire, Quebec, Canada), was added to 100 µl aliquots of tumor cells (10^7 cells/ml), which were then drawn into glass capillary tubes. Tubes were sealed, placed into quartz EPR tubes, and samples were kept at 37°C. The EPR linewidth reports on pO_2, so oxygen consumption rates were obtained by measuring the pO_2 in the closed tubes over time and determining the slope of the resulting linear plot (Diepart et al., 2010). Mitochondrial oxygen consumption was determined by paired measurements ± 1 µM rotenone. The dose-dependent effect of rotenone on oxygen consumption (Figure S4A) was determined using MitoXpress (Luxcel Biosciences), according to the manufacturer's protocol.

Metabolite and ATP determination

In all assays, an equal amount of cells was plated to adhere for 24h in DMEM without glutamine, pyruvate and serum. Lactate, glucose and pyruvate concentrations were measured on deproteinized cell supernatants using a CMA600 analyzer as previously described (Sonveaux et al., 2012). Intracellular succinate and 2-oxoglutarate levels were measured in deproteinized cell lysates collected in RIPA buffer using enzymatic assays from Roche and Source Bioscience, respectively. ATP was measured in cells after an 8-h treatment with the indicated drugs using ATP bioluminescent somatic assay kit (Sigma) as previously described (Sonveaux et al., 2008).

ROS measurements

MitoSOX was used to measure superoxide levels according to manufacturer's instructions (Invitrogen). Signals were measured in 50,000 cells on FACSCalibur (BD) following a 6-h treatment. Data were presented in the FL2 channel (585/42 nm) and analyzed with the FlowJo software (Tree Star). For total ROS measurements, 20,000 cells/well were incubated with 1 µM CM-H_2DCFDA (Invitrogen) in PBS for 30 min. Fluorescence was measured using a Victor X4 plate reader (Perkin Elmer; λ_{ex} = 490 nm, λ_{em} = 535 nm). Protein content was quantified following Bradford's dosage after lysis.

RNA interference and lentiviral preparation

Control (EHUEGFP), *mt-CO1* (EHU117481) and *SMAD4* (EMU016021) endoribonuclease-prepared (e)siRNAs were from Sigma. For human cells, control siRNA was Allstar (Qiagen) and siRNA against human *PYK2* (SASI_Hs01_00032249) was from Sigma. For murine cells, ON-TARGETplus SMARTpool control siRNAs and SMARTpool murine siRNAs against *Pyk2* were from ThermoScientific. All siRNAs and esiRNAs were transfected with RNAi/MAX according to manufacturer's instructions (Invitrogen). pLKO.1 lentiviral vectors expressing control shRNA (Addgene 1864), mouse *Uqcrb* shRNAs (shRNA-1: clone TRCN0000042310, shRNA-2: clone TRCN0000042311; ThermoScientific) and mouse *Ptk2b/Pyk2* shRNA (shRNA-1: clone TRCN0000023632 and shRNA-2 TRCN0000023631; ThermoScientific) were used to generate viral particles with the lentiviral packaging mix (Sigma) according to the manufacturer's instructions. For lentivirus preparation, HEK293FT cells were transiently transfected with lipofectamine using a third-generation lentiviral system as described (Moon et al., 2010). After 24h and 48h, viral supernatants were harvested, titrated, and used to infect target cells. Selection was with puromycin (2 µg/mL).

Metabolic metastasis

Microarrays

To identify a prometastatic gene expression signature, we compared the whole genome expression of 3 independent cultures of wild-type B16F10 mouse melanoma cells to that of B16-M2a, B16-M4b, and B16F10 cells treated with 10 nM of rotenone for 6 hours. Total RNA was collected from cell lysate in Tri-Reagent (Molecular Research Center) following manufacturer's instructions. Whole genome expression was performed at Arraystar using the mouse 4x44K Gene Expression Array (Agilent) for hybridization, the GeneSpring GX v12.0 software (Agilent) for quantile normalization and data processing, and Agilent Feature Extraction software (version 11.0.1.1) for data analysis. Differentially expressed genes between two samples were identified after 1.5-fold change filtering. The gene signature shared between all three subsets was determined using volcano plot filtering and paired Student's *t* test.

RT-qPCR, immunoblotting and cell fractionation

For RT-qPCR, total RNA was collected from cell lysate in Tri-Reagent (Molecular Research Center) following manufacturer's instructions. RT was performed using RevertAid M-MuLV reverse transcriptase and random hexamer primers (Fermentas) followed by SYBR green qPCR as previously shown (Bouzin et al., 2007). Primers were: human *MT-CO1* sense 5'-GGCCTGACTGGCATTGTATT-3', antisense 5'-TGGCGTAGGTTTGGTCTAGG-3'; human *RPL19* sense 5'-CAAGCGGATCTCATGGAACA-3', antisense 5'-TGGTCAGCCAGGAGCTTCTT-3'; mouse *Ptk2b*/*Pyk2* sense 5'-ATCTTGACCACCCTCACATCG-3', antisense 5'-TAGTGTCCCAGCTCCCCATAA-3'; and mouse *Actb*/*β-actin* sense 5'-GGCTGTATTCCCCTCCATCG-3', antisense 5'-CCAGTTGGTAACAATGCCATGT-3'. A previously disclosed protocol was used for Western Blotting (Feron et al., 1996). For the detection of Src phosphorylation in mitochondria, mitochondrial protein fraction isolation was performed as reported by Rasola et al. (2010). Primary antibodies were mouse monoclonals against MT-CO1 (Invitrogen) or β-actin (Sigma-Aldrich), and rabbit polyclonals against Src (Cell Signaling), P-Y416-Src (Cell Signaling), Pyk2 (Cell Signaling), SMAD4 (B-8, SantaCruz), P-Y402-Pyk2 (SantaCruz), or UQCRB (Proteintech).

Metastatic take and spontaneous metastasis assays

For metastatic take assays, B16F10-Luc, B16F10-Luc-shCTR or B16F10-Luc-shRNA-1-UQCRB cells were pretreated for 6h with the indicated drugs then resuspended in HBSS. 10^6 viable cells were injected into the tail vein of syngeneic 8 week-old C57BL/6j mice. Mice were sacrificed at first detection of a bioluminescence signal with an IVIS50 (Xenogen) upon 150 mg/kg luciferin injection. The number of mestastatic lesions was determined under a stereoscopic microscope. Same conditions were applied with B16-M4b. For spontaneous metastasis assays with B16F10-M4b, tumor cells were injected subcutaneously to mice, as described above for the generation of supermetastatic cells. For spontaneous metastasis with MDA-MB-231-LUC-D3H2LN cells, 10^6 tumor cells were injected orthotopically into the mammary fat pad of SCID mice (Charles Rivers). In these two assays, where indicated, mice were treated daily with mitoTEMPO (0.7 mg/kg) or vehicle. Primary tumors were removed when reaching a diameter of approximately 1 cm, i.e. after ~12 days for B16F10-M4b and ~5 weeks for MDA-MB231-D3H2-LUC2 (Gabri et al., 2006; Sossey-Alaoui et al., 2007). In the B16 model, mice were sacrificed one month after primary tumor implantation and lung metastases were counted under a stereoscopic microscope. In the MDA-MB-231 model, mice were sacrificed two months after primary tumor implantation, *ex vivo* bioluminescence signals were acquired in the presence of 2.5 mg/ml luciferin and used to quantify metastatic dissemination (Kim et al., 2008). Primary tumor

volume was calculated using the formula of a prolate ellipsoid following measurements with an electronic caliper (De Saedeleer et al., 2012).

SUPPLEMENTAL REFERENCES

De Saedeleer, C.J., Copetti, T., Porporato, P.E., Verrax, J., Feron, O., and Sonveaux, P. (2012). Lactate Activates HIF-1 in Oxidative but Not in Warburg-Phenotype Human Tumor Cells. PLoS. ONE. *7*, e46571.

Diepart, C., Verrax, J., Calderon, P.B., Feron, O., Jordan, B.F., and Gallez, B. (2010). Comparison of methods for measuring oxygen consumption in tumor cells in vitro. Anal. Biochem. *396*, 250-256.

Feron, O., Belhassen, L., Kobzik, L., Smith, T.W., Kelly, R.A., and Michel, T. (1996). Endothelial nitric oxide synthase targeting to caveolae. Specific interactions with caveolin isoforms in cardiac myocytes and endothelial cells. J. Biol. Chem. *271*, 22810-22814.

Filigheddu, N., Cutrupi, S., Porporato, P.E., Riboni, F., Baldanzi, G., Chianale, F., Fortina, E., Piantanida, P., De, B.M., Vacca, G. et al. (2007). Diacylglycerol kinase is required for HGF-induced invasiveness and anchorage-independent growth of MDA-MB-231 breast cancer cells. Anticancer Res. *27*, 1489-1492.

Gabri, M.R., Mazorra, Z., Ripoll, G.V., Mesa, C., Fernandez, L.E., Gomez, D.E., and Alonso, D.F. (2006). Complete antitumor protection by perioperative immunization with GM3/VSSP vaccine in a preclinical mouse melanoma model. Clin. Cancer Res. *12*, 7092-7098.

Kim, S.Y., Lee, C.H., Midura, B.V., Yeung, C., Mendoza, A., Hong, S.H., Ren, L., Wong, D., Korz, W., Merzouk, A. et al. (2008). Inhibition of the CXCR4/CXCL12 chemokine pathway reduces the development of murine pulmonary metastases. Clin. Exp. Metastasis *25*, 201-211.

Moon, E.J., Sonveaux, P., Porporato, P.E., Danhier, P., Gallez, B., Batinic-Haberle, I., Nien, Y.C., Schroeder, T., and Dewhirst, M.W. (2010). NADPH oxidase-mediated reactive oxygen species production activates hypoxia-inducible factor-1 (HIF-1) via the ERK pathway after hyperthermia treatment. Proc. Natl. Acad. Sci. U. S. A *107*, 20477-20482.

Rasola, A., Sciacovelli, M., Chiara, F., Pantic, B., Brusilow, W.S., and Bernardi, P. (2010). Activation of mitochondrial ERK protects cancer cells from death through inhibition of the permeability transition. Proc. Natl. Acad. Sci. U. S. A *107*, 726-731.

Sonveaux, P., Copetti, T., De Saedeleer, C.J., Vegran, F., Verrax, J., Kennedy, K.M., Moon, E.J., Dhup, S., Danhier, P., Frerart, F. et al. (2012). Targeting the lactate transporter MCT1 in endothelial cells inhibits lactate-induced HIF-1 activation and tumor angiogenesis. PLoS. ONE. *7*, e33418.

Sossey-Alaoui, K., Safina, A., Li, X., Vaughan, M.M., Hicks, D.G., Bakin, A.V., and Cowell, J.K. (2007). Down-regulation of WAVE3, a metastasis promoter gene, inhibits invasion and metastasis of breast cancer cells. Am. J. Pathol. *170*, 2112-2121.